

Size-effects of metamaterial beams subjected to pure bending: on boundary conditions and parameter identification in the relaxed micromorphic model

Mohammad Sarhil^{1,*}, Lisa Scheunemann², Jörg Schröder¹ and Patrizio Neff³

¹Institute of Mechanics, University of Duisburg-Essen
Universitätsstr. 15, 45141 Essen, Germany
e-mail: mohammad.sarhil@uni-due.de

²Chair of Applied Mechanics, Gottlieb-Daimler-Str., TU Kaiserslautern,
67663 Kaiserslautern, Germany

³Chair of Nonlinear Analysis and Modeling, Faculty of Mathematics,
Thea-Leymann-Str. 9, University of Duisburg-Essen,
45141 Essen, Germany

Abstract

We devote this paper to model the size-effects of metamaterial beams under bending with the aid of the relaxed micromorphic continuum. We analyze first the size-dependent bending stiffness of heterogeneous fully discretized metamaterial beams subjected to pure bending loads. Two equivalent loading schemes are introduced which lead to a constant moment along the beam length with no shear force. The relaxed micromorphic model is employed then to retrieve the size-effects. We present a procedure for the determination of the material parameters of the relaxed micromorphic model based on the fact that the model operates between two well-defined scales. These scales are given by linear elasticity with micro and macro elasticity tensors which bound the relaxed micromorphic continuum from above and below, respectively. The micro elasticity tensor is specified as the maximum possible stiffness that is exhibited by the assumed metamaterial while the macro elasticity tensor is given by standard periodic first-order homogenization. For the identification of the micro elasticity tensor, two different approaches are shown which rely on affine and non-affine Dirichlet boundary conditions of candidate unit cell variants with the possible stiffest response. The consistent coupling condition is shown to allow the model to act on the whole intended range between macro and micro elasticity tensors for both loading cases. Finally, we fit the relaxed micromorphic model against the fully resolved metamaterial solution by controlling the curvature magnitude after linking it with the specimen's size.

Keywords: size-effects, consistent coupling condition, metamaterials, relaxed micromorphic model, generalized continua, homogenization.

1. Introduction

Mechanical metamaterials are unconventional materials with exotic mechanical properties that are governed by the geometry of the complex underlying microstructure rather than by the properties of the constituting materials [29, 36, 50, 101, 102]. They can be optimized to obtain the intended mechanical properties to fit the wanted functionality [94]. However, mechanical metamaterials typically reveal size-effect phenomena and therefore the classical Cauchy-Boltzmann theory and first-order homogenization methods are incapable to describe such mechanical behavior. Generalized continua are enhanced continua that can model these metamaterials as a homogeneous continuum without accounting for the detailed microstructure. The enhancement can be achieved by expanding the kinematics to contain additional degrees of freedom, e.g. the classical micromorphic theory [26, 27, 40, 58, 93] and the Cosserat theory [9, 19, 51, 62, 63], or by accounting for higher-grade differential operators in the energy functional, e.g. gradient elasticity models [5, 11–13, 25, 28, 35, 59, 86, 98]. However, the identification of the material parameters of these models is not trivial and in general unsolved. Different schemes were presented for the homogenization of the heterogeneous fully resolved microstructures into the Cosserat continuum in [9, 31, 39, 69], different variants of the gradient elasticity continuum in [2, 3, 14, 42, 48, 83, 88, 95–97, 99] and the fully micromorphic continuum in [8, 16, 30, 38, 78–80, 103], however, without leading to a universally accepted answer.

The relaxed micromorphic model is a generalized continuum model that allows in principle to capture size-effects and to describe band gaps phenomena in the dynamical case, see for example [6, 15, 20, 23, 54–57, 73, 75, 75, 76]. This model has been introduced in [32, 64] and its well-posedness for the static and dynamic problems has been proved in [65, 67]. In [46] the regularity of the model was investigated. Being a micromorphic model, it features the classical translational degrees of freedom $\mathbf{u} : \mathcal{B} \in \mathbb{R}^3 \rightarrow \mathbb{R}^3$ as well

as a non-symmetric micro-distortion field $\mathbf{P} : \mathcal{B} \in \mathbb{R}^3 \rightarrow \mathbb{R}^{3 \times 3}$. Compared to the classical micromorphic approach, the assumed strain energy is drastically simplified; notably, the curvature part (derivatives of \mathbf{P}) intervenes only through $\text{Curl } \mathbf{P}$, so that solutions are found in $H^1(\mathcal{B}) \times H(\text{curl}, \mathcal{B})$ for the pair (\mathbf{u}, \mathbf{P}) . Using only the Curl of \mathbf{P} has some decisive advantages. It generates "bounded stiffness" [70–72, 74] for arbitrary large characteristic length (arbitrary small samples), in opposition to all strain gradient or classical micromorphic approaches. Moreover, the appearing length-scale independent elasticity tensors \mathbb{C}_e and $\mathbb{C}_{\text{micro}}$ are related by the Reuss-like homogenization formula

$$\mathbb{C}_e = \mathbb{C}_{\text{micro}}(\mathbb{C}_{\text{micro}} - \mathbb{C}_{\text{macro}})^{-1}\mathbb{C}_{\text{macro}}, \quad (1)$$

where $\mathbb{C}_{\text{macro}}$ is uniquely known from classical periodic homogenization. It remains to determine $\mathbb{C}_{\text{micro}}$, which happens to be the largest observable stiffness in the model (such an identification does not exist for the classical micromorphic model or other variants of it). As it turns out, the relaxed micromorphic model interpolates between two well-defined scales: the classical continuum scales of macroscopic elasticity, whose stiffness is given by $\mathbb{C}_{\text{macro}}$ and a microscopic scale, with stiffness $\mathbb{C}_{\text{micro}}$. The role of the characteristic length $L_c > 0$ is then to scale correctly with the size of the specimen and to describe the interaction between the two scales. For $L_c \rightarrow 0$ we recover macroscopic elasticity and for $L_c \rightarrow \infty$ (zoom into the microstructure) we obtain the microscopic scale (stiffness $\mathbb{C}_{\text{micro}}$). In this contribution, we want to explore the possibilities that this unique interpretation of the relaxed micromorphic model provides. We consider an architected material (hard matrix with soft inclusions). The determination of $\mathbb{C}_{\text{macro}}$ is a standard identification in periodic homogenization theory. The identification of $\mathbb{C}_{\text{micro}}$ will be guided by the largest stiffness idea. Therefore, we consider a bending test of slender metamaterial beams. The size-dependent bending was analyzed by means of other enriched models such as strain gradient, micropolar and others continua in [4, 7, 37, 41–43, 49, 52, 53, 100]. Modeling the mechanical behavior of many metamaterials was achieved for a variety of applications using generalized continua in [1, 18, 22, 24, 34, 68, 81, 85, 87, 91, 92].

In this work the size-effects of metamaterial beams with fully discretized microstructure are analyzed. Afterward, we employ the relaxed micromorphic continuum to describe these size-effects without accounting for the detailed microstructure. The material parameters and adequate boundary conditions of the micro-distortion field should be identified in order to establish a simplified fitting procedure on the fully resolved metamaterial beams. The so-called consistent coupling condition (applied on the Dirichlet boundary for \mathbf{u}) allows the relaxed micromorphic to operate on the whole scale between $\mathbb{C}_{\text{macro}}$ and $\mathbb{C}_{\text{micro}}$ which is of pivotal importance for a correct identification of the material parameters. However, an alternative loading by a normal linear traction (applied moment), which delivers the exactly the same results for the fully resolved metamaterial, achieves consistent results as well for the relaxed micromorphic model when the consistent coupling condition is imposed via the penalty approach on the part of the boundary where the traction is set.

In a previous attempt [66] $\mathbb{C}_{\text{micro}}$ was supposed to be given by the Löwner matrix supremum $\mathbb{C}_{\text{micro}}^{\text{Löwner}}$ of elasticity tensors appearing under affine Dirichlet conditions on the unit-cell level. From the results in the present paper it inspires that $\mathbb{C}_{\text{micro}}^{\text{Löwner}}$ is too soft, when compared with the appearing stiffness in the bending regime. Here, we extend our understanding of $\mathbb{C}_{\text{micro}}$ towards all scenarios, notably including non-affine Dirichlet conditions. We limit our consideration to the planar case, in which the isotropic curvature energy in terms of $\text{Curl } \mathbf{P}$ has only one free parameter.

The outline of the paper is as follows: in Section 2 we recall the energy functional of the relaxed micromorphic model, define the material parameters, and introduce the strong forms with the associated boundary conditions obtained by the energy minimization. We present briefly in Section 3 the main aspects of the construction of $H(\text{curl}, \mathcal{B})$ -conforming finite elements. The size-effects of the heterogeneous micro-structured metamaterial beams are investigated in Section 4 for two loading cases which lead to the same results. In Section 5 we determine the material parameters of the relaxed micromorphic model and discuss the boundary condition for symmetric and non-symmetric force stresses. We then fit the relaxed micromorphic model solution to the micro-structured metamaterial solution by calibrating the curvature in Section 6. Finally, we provide our conclusions and outlook in Section 7.

2. The relaxed micromorphic model

The relaxed micromorphic model (RMM) is an enriched continuum model. The kinematics of each material point is determined, similar to the general micromorphic theory [27, 58, 93], by a displacement vector

$\mathbf{u}: \mathcal{B} \subseteq \mathbb{R}^3 \rightarrow \mathbb{R}^3$ and a non-symmetric micro-distortion field $\mathbf{P}: \mathcal{B} \subseteq \mathbb{R}^3 \rightarrow \mathbb{R}^{3 \times 3}$. The displacement and the micro-distortion fields are defined for the static case by minimizing the energy functional

$$\Pi(\mathbf{u}, \mathbf{P}) = \int_{\mathcal{B}} W(\nabla \mathbf{u}, \mathbf{P}, \text{Curl } \mathbf{P}) - \bar{\mathbf{f}} \cdot \mathbf{u} \, dV - \int_{\partial \mathcal{B}_t} \bar{\mathbf{t}} \cdot \mathbf{u} \, dA \longrightarrow \min, \quad (2)$$

with $(\mathbf{u}, \mathbf{P}) \in H^1(\mathcal{B}) \times H(\text{curl}, \mathcal{B})$. The vector $\bar{\mathbf{f}}$ describes the applied body force. The vector $\bar{\mathbf{t}}$ is the traction vector acting on the boundary $\partial \mathcal{B}_t \subset \partial \mathcal{B}$. The elastic energy density W reads

$$\begin{aligned} W(\nabla \mathbf{u}, \mathbf{P}, \text{Curl } \mathbf{P}) = & \frac{1}{2} (\text{sym}[\nabla \mathbf{u} - \mathbf{P}] : \mathbb{C}_e : \text{sym}[\nabla \mathbf{u} - \mathbf{P}] + \text{sym } \mathbf{P} : \mathbb{C}_{\text{micro}} : \text{sym } \mathbf{P} \\ & + \text{skew}[\nabla \mathbf{u} - \mathbf{P}] : \mathbb{C}_c : \text{skew}[\nabla \mathbf{u} - \mathbf{P}] + \mu L_c^2 \text{Curl } \mathbf{P} : \mathbb{L} : \text{Curl } \mathbf{P}). \end{aligned} \quad (3)$$

Here, $\mathbb{C}_{\text{micro}}, \mathbb{C}_e > \mathbf{0}$ are fourth-order positive definite standard elasticity tensors, $\mathbb{C}_c \geq \mathbf{0}$ is a fourth-order positive semi-definite rotational coupling tensor, \mathbb{L} is a fourth-order tensor, $L_c \geq 0$ is the characteristic length parameter and μ is a shear modulus. The characteristic length parameter is related to the size of the microstructure and determines its influence on the macroscopic mechanical behavior. The characteristic length allows to scale the number of considered unit cells keeping all remaining parameters of the model scale-independent where the macro-scale with $\mathbb{C}_{\text{macro}}$ and the micro-scale with $\mathbb{C}_{\text{micro}}$ are retrieved for $L_c \rightarrow 0$ and $L_c \rightarrow \infty$, respectively, if suitable boundary conditions are applied, see [66, 84]. The constitutive coefficients are assumed constant with the following symmetries

$$\begin{aligned} (\mathbb{C}_{\text{micro}})_{ijkl} &= (\mathbb{C}_{\text{micro}})_{klij} = (\mathbb{C}_{\text{micro}})_{jikl}, & (\mathbb{C}_c)_{ijkl} &= (\mathbb{C}_c)_{klij}, \\ (\mathbb{C}_e)_{ijkl} &= (\mathbb{C}_e)_{klij} = (\mathbb{C}_e)_{jikl}, & (L_c)_{ijkl} &= (L_c)_{klij}. \end{aligned} \quad (4)$$

The variation of the potential with respect to the displacement yields the weak form

$$\delta_{\mathbf{u}} \Pi = \int_{\mathcal{B}} \underbrace{\{\mathbb{C}_e : \text{sym}[\nabla \mathbf{u} - \mathbf{P}] + \mathbb{C}_c : \text{skew}[\nabla \mathbf{u} - \mathbf{P}]\}}_{=: \boldsymbol{\sigma}} : \nabla \delta \mathbf{u} - \bar{\mathbf{f}} \cdot \delta \mathbf{u} \, dV - \int_{\partial \mathcal{B}_t} \bar{\mathbf{t}} \cdot \delta \mathbf{u} \, dA = 0, \quad (5)$$

which leads, using integration by parts and employing the divergence theorem, to

$$\delta_{\mathbf{u}} \Pi = \int_{\mathcal{B}} \{\text{div } \boldsymbol{\sigma} + \bar{\mathbf{f}}\} \cdot \delta \mathbf{u} \, dV = 0, \quad (6)$$

where $\boldsymbol{\sigma}$ is the non-symmetric force stress tensor (symmetric if $\mathbb{C}_c \equiv \mathbf{0}$ which is permitted). In a similar way, the variation of the potential with respect to the micro-distortion field \mathbf{P} leads to the weak form

$$\delta_{\mathbf{P}} \Pi = \int_{\mathcal{B}} \underbrace{\{\boldsymbol{\sigma} - \mathbb{C}_{\text{micro}} : \text{sym } \mathbf{P} + \bar{\mathbf{M}}\}}_{=: \boldsymbol{\sigma}_{\text{micro}}} : \delta \mathbf{P} - \underbrace{\mu L_c^2 (\mathbb{L} : \text{Curl } \mathbf{P})}_{=: \mathbf{m}} : \text{Curl } \delta \mathbf{P} \, dV = 0, \quad (7)$$

which can be rewritten, using integration by parts and applying Stokes' theorem, as

$$\delta_{\mathbf{P}} \Pi = \int_{\mathcal{B}} \{\boldsymbol{\sigma} - \boldsymbol{\sigma}_{\text{micro}} - \text{Curl } \mathbf{m}\} : \delta \mathbf{P} \, dV + \int_{\partial \mathcal{B}} \left\{ \sum_{i=1}^3 (\mathbf{m}^i \times \delta \mathbf{P}^i) \cdot \mathbf{n} \right\} \, dA = 0, \quad (8)$$

where the stress measurements $\boldsymbol{\sigma}_{\text{micro}}$ and \mathbf{m} are the micro- and moment stresses, respectively, \mathbf{n} is the outward unit normal vector on the boundary, and \mathbf{m}^i and $\delta \mathbf{P}^i$ are the row vectors of the related second-order tensors. The strong form of the relaxed micromorphic model with the associated boundary conditions read

$$\text{div } \boldsymbol{\sigma} + \bar{\mathbf{f}} = \mathbf{0} \quad \text{on } \mathcal{B}, \quad (9a)$$

$$\mathbf{u} = \bar{\mathbf{u}} \quad \text{on } \partial \mathcal{B}_u, \quad (9b)$$

$$\bar{\mathbf{t}} = \boldsymbol{\sigma} \cdot \mathbf{n} \quad \text{on } \partial \mathcal{B}_t, \quad (9c)$$

$$\boldsymbol{\sigma} - \boldsymbol{\sigma}_{\text{micro}} - \text{Curl } \mathbf{m} = \mathbf{0} \quad \text{on } \mathcal{B}, \quad (9d)$$

$$\sum_{i=1}^3 \mathbf{P}^i \times \mathbf{n} = \bar{\mathbf{t}}_p \quad \text{on } \partial \mathcal{B}_p, \quad (9e)$$

$$\sum_{i=1}^3 \mathbf{m}^i \times \mathbf{n} = \mathbf{0} \quad \text{on } \partial \mathcal{B}_m, \quad (9f)$$

where $\partial\mathcal{B}_P \cap \partial\mathcal{B}_m = \partial\mathcal{B}_u \cap \partial\mathcal{B}_t = \emptyset$ and $\partial\mathcal{B}_P \cup \partial\mathcal{B}_m = \partial\mathcal{B}_u \cup \partial\mathcal{B}_t = \partial\mathcal{B}$. The strong form represents a generalized balance of linear momentum (force balance) and a generalized balance of angular momentum (moment balance). For more details regarding derivations of the boundary conditions, the reader is referred to [84].

An additional dependence between the displacement field and the micro-distortion field on the boundary was proposed in [66] and subsequently considered in [21, 70, 71, 89]. This so-called **consistent coupling condition** is defined by

$$\mathbf{P} \cdot \boldsymbol{\tau} = \nabla \mathbf{u} \cdot \boldsymbol{\tau} \Leftrightarrow \mathbf{P}^i \times \mathbf{n} = \nabla \mathbf{u}^i \times \mathbf{n} \quad \text{for } i = 1, 2, 3 \quad \text{on } \partial\mathcal{B}_P = \partial\mathcal{B}_u, \quad (10)$$

where $\boldsymbol{\tau}$ is the tangential vector on the boundary and \mathbf{P}_i and $\nabla \mathbf{u}^i$ are the row-vectors of the associated tensors. However, we can extend this relative boundary condition to parts of \mathcal{B}_m by enforcing the consistent coupling condition on $\partial\mathcal{B}_{\widehat{m}} \subseteq \partial\mathcal{B}_m$ via a penalty approach as

$$\Pi \Leftarrow \Pi + \int_{\partial\mathcal{B}_{\widehat{m}}} \frac{\kappa_1}{2} \sum_{i=1}^3 \|(\mathbf{P}^i - \nabla \mathbf{u}^i) \times \mathbf{n}\|^2 dA, \quad (11)$$

where κ_1 is the penalty parameter.

The micro-distortion field has the following general form for the three-dimensional case

$$\mathbf{P} = \begin{pmatrix} (\mathbf{P}^1)^T \\ (\mathbf{P}^2)^T \\ (\mathbf{P}^3)^T \end{pmatrix} = \begin{pmatrix} P_{11} & P_{12} & P_{13} \\ P_{21} & P_{22} & P_{23} \\ P_{31} & P_{32} & P_{33} \end{pmatrix} \quad \text{with } \mathbf{P}^i = \begin{pmatrix} P_{i1} \\ P_{i2} \\ P_{i3} \end{pmatrix} \quad \text{for } i = 1, 2, 3. \quad (12)$$

We let the Curl operator act on the row vectors of the micro-distortion field \mathbf{P} as

$$\text{Curl } \mathbf{P} = \begin{pmatrix} (\text{curl } \mathbf{P}^1)^T \\ (\text{curl } \mathbf{P}^2)^T \\ (\text{curl } \mathbf{P}^3)^T \end{pmatrix} = \begin{pmatrix} P_{13,2} - P_{12,3} & P_{11,3} - P_{13,1} & P_{12,1} - P_{11,2} \\ P_{23,2} - P_{22,3} & P_{21,3} - P_{23,1} & P_{22,1} - P_{21,2} \\ P_{33,2} - P_{32,3} & P_{31,3} - P_{33,1} & P_{32,1} - P_{31,2} \end{pmatrix}. \quad (13)$$

3. $H^1(\mathcal{B}) \times H(\text{curl}, \mathcal{B})$ finite element in 2D

Different finite element formulations of the relaxed micromorphic model were introduced for the plane strain case in [82, 84], antiplane shear in [89] and 3D case in [90]. For the two-dimensional case, the micro-distortion field has only four non-vanishing components, which are in the plane, and its Curl operator is reduced to only two components out of the plane, namely $(\text{Curl } \mathbf{P})_{13}$ and $(\text{Curl } \mathbf{P})_{23}$,

$$\mathbf{P} = \begin{pmatrix} (\mathbf{P}^1)^T \\ (\mathbf{P}^2)^T \\ \mathbf{0}^T \end{pmatrix} = \begin{pmatrix} P_{11} & P_{12} & 0 \\ P_{21} & P_{22} & 0 \\ 0 & 0 & 0 \end{pmatrix} \quad \text{and} \quad \text{Curl } \mathbf{P} = \begin{pmatrix} 0 & 0 & P_{12,1} - P_{11,2} \\ 0 & 0 & P_{22,1} - P_{21,2} \\ 0 & 0 & 0 \end{pmatrix}. \quad (14)$$

It has been shown in [84] that $H^1(\mathcal{B}) \times H(\text{curl}, \mathcal{B})$ elements obtain the discontinuous solution of the micro-distortion field while the standard nodal $H^1(\mathcal{B}) \times H^1(\mathcal{B})$ elements are unable to capture the jumps. Therefore, transition zones emerge for $H^1(\mathcal{B}) \times H^1(\mathcal{B})$ elements which need to be resolved by distinctly refining the mesh in contrast to $H^1(\mathcal{B}) \times H(\text{curl}, \mathcal{B})$ elements which exhibit faster convergences rates.

We demonstrate briefly the main aspects of the finite element formulation of a quadrilateral element $(\mathbf{u}, \mathbf{P}) \in H^1(\mathcal{B}) \times H(\text{curl}, \mathcal{B})$ shown in Figure 1. The finite element, denoted as Q2NQ2, utilizes Lagrange-type shape functions of the second-order for the displacement field, denoted as Q2. The suitable finite element space for the micro-distortion field is known as Nédélec space, see [60, 61]. In this work, we choose the Nédélec space of first-kind and second-order, denoted as NQ2. Nédélec formulation uses vectorial shape functions that satisfy the tangential continuity at element interfaces. General reviews about the edge elements are available in [45] and [77]. For more details regarding the derivation of shape functions and the FEM-implementation aspects, the reader is referred to [84].

The Q2NQ2 element uses 9 nodes for the discretization of the displacement field \mathbf{u} . The geometry and the displacement field are approximated employing the related quadratic scalar shape functions N_i^u defined

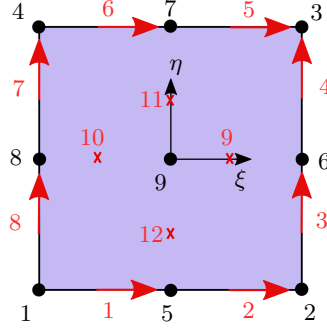


Figure 1: Q2NQ2 Element. Black dots represent the displacement nodes. Red arrows and crosses indicate the edge and inner vectorial dofs, respectively, of the micro-distortion field used in Nédélec formulation.

in the parameter space with natural coordinates $\boldsymbol{\xi} = \{\xi, \eta\}$ by

$$\mathbf{X}_h = \sum_{I=1}^9 N_I^u(\boldsymbol{\xi}) \mathbf{X}_I, \quad \mathbf{u}_h = \sum_{I=1}^9 N_I^u(\boldsymbol{\xi}) \mathbf{d}_I^u, \quad (15)$$

where \mathbf{X}_I are the coordinates of the displacement node I and \mathbf{d}_I^u are its displacement degrees of freedom. The deformation gradient is obtained then in physical space by

$$\nabla \mathbf{u}_h = \sum_{I=1}^9 \mathbf{d}_I^u \otimes \nabla N_I^u(\boldsymbol{\xi}), \quad \text{with} \quad \nabla N_I^u(\boldsymbol{\xi}) = \mathbf{J}^{-T} \cdot \nabla_{\boldsymbol{\xi}} N_I^u, \quad (16)$$

where $\mathbf{J} = \frac{\partial \mathbf{X}}{\partial \boldsymbol{\xi}}$ is the Jacobian, ∇ and $\nabla_{\boldsymbol{\xi}}$ are the gradient operators to \mathbf{X} and $\boldsymbol{\xi}$, respectively. Regarding the micro-distortion field, Nédélec quadrilateral finite elements of the first type and order k are based on the space

$$\left[\mathcal{ND}^{\square} \right]_k^2 = \left[\begin{array}{c} Q_{k-1,k} \\ Q_{k,k-1} \end{array} \right] \quad \text{where} \quad Q_{m,n} = \text{span}\{\xi^i \eta^j \mid i \leq m, j \leq n\}, \quad (17)$$

with $\dim \left(\left[\mathcal{ND}^{\square} \right]_k^2 \right) = 2k(k+1)$. The vectorial shape functions \mathbf{v}^k in parametric space are obtained by constructing a linear system of equations defined using a set of inner and outer dofs. The outer dofs of an edge e_i are defined by the integral

$$m_j^{e_i}(\mathbf{v}^k) = \int_{e_i} (\mathbf{v}^k \cdot \mathbf{t}_i) r_j ds, \quad \forall r_j \in \mathbb{P}_{k-1}(e_i) \quad (18)$$

where \mathbf{t}_i is the normalized tangential vector of the edge e_i and r_j is a polynomial \mathbb{P}_{k-1} defined along the edge e_i where \mathbb{P}_{k-1} is the linear space of polynomials of degree $k-1$ or less. The inner dofs are introduced as

$$m_i^{\text{inner}}(\mathbf{v}^k) = \int_{\mathcal{B}_e} \mathbf{v}^k \cdot \mathbf{q}_i da, \quad \forall \mathbf{q}_i \in \left[\begin{array}{c} Q_{k-1,k-2}(\mathcal{B}_e) \\ Q_{k-2,k-1}(\mathcal{B}_e) \end{array} \right], \quad (19)$$

where the scalar-valued and vectorial functions r_j and \mathbf{q}_i are linearly independent polynomials which are chosen as Lagrange polynomials. In total, we have $4k$ edge dofs and $2k(k-1)$ inner dofs and the sum equals to $2k(k+1)$ which is the space dimension. For our second-order element ($k=2$), we have 8 edge and 4 inner dofs. The derivations of the $H(\text{curl}, \mathcal{B})$ -conforming vectorial shape functions is shown in details in [84]. Mapping the vectorial shape functions from \mathbf{v}_I^2 in the parametric space to $\boldsymbol{\psi}_I^2$ in the physical space must conserve the tangential continuity property. This is achieved by the so-called covariant Piola transformation, see for example [77], which reads

$$\hat{\boldsymbol{\psi}}_I^2 = \mathbf{J}^{-T} \cdot \mathbf{v}_I^2 \quad \text{and} \quad \text{curl} \hat{\boldsymbol{\psi}}_I^2 = \frac{1}{\det \mathbf{J}} \mathbf{J} \cdot \text{curl}_{\boldsymbol{\xi}} \mathbf{v}_I^2. \quad (20)$$

For our implementation, we modify the mapping to the form

$$\boldsymbol{\psi}_I^2 = \alpha_I \beta_I \hat{\boldsymbol{\psi}}_I^2 \quad \text{and} \quad \text{curl} \boldsymbol{\psi}_I^2 = \alpha_I \beta_I \text{curl} \hat{\boldsymbol{\psi}}_I^2. \quad (21)$$

The orientation consistency parameter $\alpha_I = \pm 1$ ensures the compatibility of the shape vectors on the edges shared by two elements in physical space. The parameter β_I is a normalization parameter which equals $L_I/2$ for $k = 2$ where L_I is the length of the related edge in physical space. It enforces that the sum of the vectorial shape functions at a common edge scalar multiplied with the associated tangential vector has to be equal one in physical space. Moreover, their scalar product with the tangential vector of the other edges must vanish, see [84] for details.

For the 2D case, the rotation of the vectorial shape functions has only one active component out of plane which reads

$$\text{curl}^{2D} \psi_I^2 = \frac{\alpha_I \beta_I}{\det \mathbf{J}} \text{curl}_{\xi}^{2D} \mathbf{v}_I^2. \quad (22)$$

The micro-distortion field \mathbf{P} is approximated by the vectorial dofs \mathbf{d}_I^P presenting its tangential components at the location $I = 1, \dots, 12$. The micro-distortion field and its Curl operator are interpolated as

$$\mathbf{P}_h = \sum_{I=1}^{12} \mathbf{d}_I^P \otimes \psi_I^2, \quad \text{Curl } \mathbf{P}_h = \sum_{I=1}^{12} \mathbf{d}_I^P \otimes \text{curl } \psi_I^2. \quad (23)$$

The non-vanishing components of the Curl operator of the micro-distortion field for the 2D case are obtained by

$$\begin{bmatrix} \text{curl}^{2D} \mathbf{P}_h^1 \\ \text{curl}^{2D} \mathbf{P}_h^2 \end{bmatrix} = \sum_{I=1}^{12} \mathbf{d}_I^P \text{curl}^{2D} \psi_I^2 = \begin{bmatrix} \sum_{I=1}^{12} (d_I^P)_1 \text{curl}^{2D} \psi_I^2 \\ \sum_{I=1}^{12} (d_I^P)_2 \text{curl}^{2D} \psi_I^2 \end{bmatrix}. \quad (24)$$

The simulations presented in this paper are performed within AceGen and AceFEM programs. The interested reader is referred to [47].

4 Reference study: size-effects of metamaterial specimens subjected to bending

We investigate here the size-effect phenomena of an assumed metamaterial with fully resolved microstructure. The size-effect phenomena will be analyzed via the effective bending stiffness of beams subjected to pure bending. According to the elementary beam theory, the moment is linked to the curvature by

$$M(x) = D(x)\kappa(x), \quad (25)$$

where $D(x)$ and $\kappa(x)$ are the bending stiffness and the curvature at a position x along the beam. For a constant bending moment \overline{M} along the beam length, we assume an effective flexural rigidity \overline{D} and an effective curvature $\overline{\kappa}$ so that we obtain

$$\overline{D} = \frac{\overline{M}}{\overline{\kappa}}. \quad (26)$$

We consider a metamaterial with a unit cell consisting of a square with an edge length $l = 1.9 \cdot 10^{-2}$ m and a circular inclusion at its center with a diameter of $d = 1.2 \cdot 10^{-2}$ m, see Figure 2. Both matrix and inclusion are isotropic linear elastic with the material parameters shown in Table 1. The inclusion is 20 times softer than the matrix. A standard triangular finite element with quadratic shape functions (T2) is used for this analysis. The specimens are considered with dimensions $H \times L = nl \times 12nl$ so the length is always twelve times the height where n is the number of unit cells in the height direction, see Figure 2.

Table 1: Material parameters of the assumed metamaterial.

	Young's modulus: E	Poisson's ratio: ν	λ	μ
Matrix	70 GPa	0.333	52.35 GPa	26.25 GPa
Inclusion	3.5 GPa	0.333	2.62 GPa	1.31 GPa

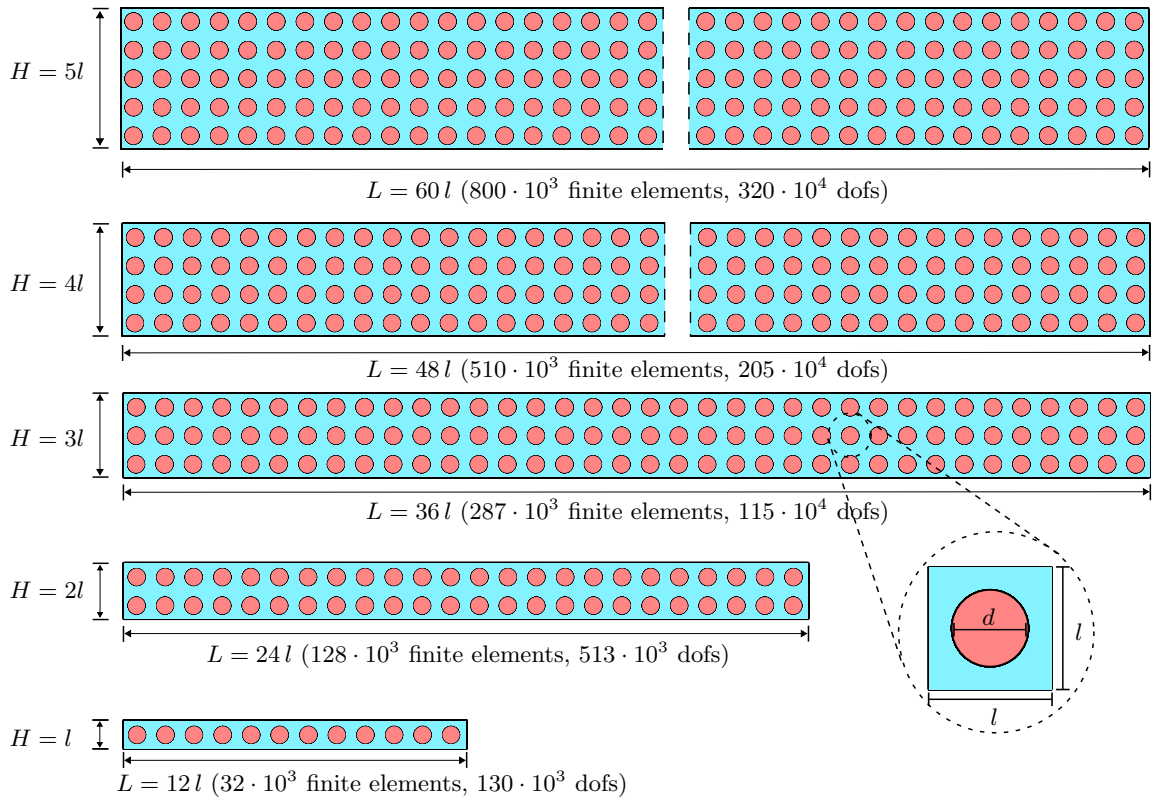


Figure 2: Illustration shows the geometry of the specimens for $n = 1, 2, 3, 4, 5$ with the assumed unit cell. The number of finite elements with degrees of freedom (dofs) are shown in parentheses.

We consider in the following two loading cases of beams subjected to pure bending without shear, see Figure 3. For the first loading case we rotate the right edge in plane through a given displacement while for the second loading case a moment is applied on the right edge by means of a traction. We intend by introducing these two loading cases to prove that they deliver identical results for the micro-structured metamaterial beams. This equivalence should be demonstrated as well by the relaxed micromorphic model when appropriate boundary conditions are set. The left boundary for both loading cases is fixed in x -direction and free to move in y -direction. We apply a rotation on the right edge with fixing the displacement in y -direction for the first loading case. For the second loading case, a traction in x -direction as a linear function of y coordinates is applied on the right edge and no displacements are allowed in y -direction, Figure 3. The equivalent beam models for the two loading cases are shown in Figure 4. Furthermore, we assume $\kappa = 1$ and $\bar{t} = 10^9$ N/m.

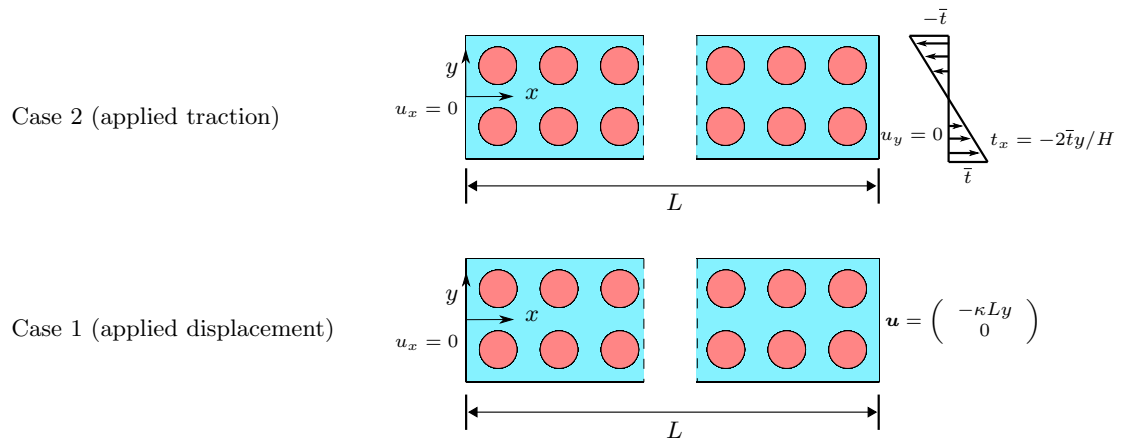


Figure 3: The boundary conditions of the fully resolved metamaterials shown exemplarily for $n = 2$ ($H \times L = 2l \times 24l$).

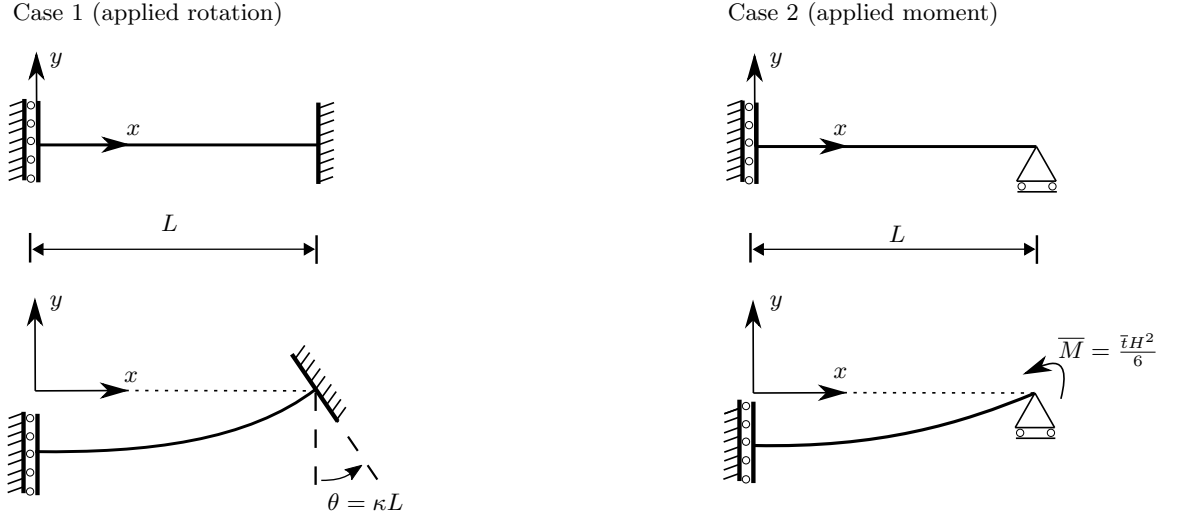


Figure 4: The equivalent beam models, compare Figure 3.

After solving the fully resolved microstructure, we introduce an effective deflection equation of the equivalent beams in Figure 4 with

$$\bar{w}(x) = \frac{\bar{\kappa}}{2}(x^2 - L^2) \quad \text{satisfying} \quad \bar{w}(L) = 0, \quad \text{and} \quad \frac{d\bar{w}(0)}{dx} = 0, \quad (27)$$

where the effective curvature $\bar{\kappa}$ is obtained by the following least square minimization

$$\sum_I^{n_{\text{node}}} (\mathbf{d}_I^u - \bar{w}(\mathbf{X}_I))^2 dx \rightarrow \min, \quad (28)$$

which leads to

$$\bar{\kappa} = \frac{\sum_I^{n_{\text{node}}} (\mathbf{d}_I^u)_2 \frac{(\mathbf{X}_I)_1^2 - L^2}{2}}{\sum_I^{n_{\text{node}}} \left(\frac{(\mathbf{X}_I)_1^2 - L^2}{2} \right)^2}, \quad (29)$$

where \mathbf{X}_I and \mathbf{d}_I^u are the coordinates and the displacement degrees of freedom at node I . The bending stiffness can be calculated following Equation 25 where the moment \bar{M} can be calculated using the nodes reactions on the left or right edges. Alternatively, the stiffness can be calculated by the deflection at the left edge of the beam as

$$\bar{D} = -\frac{\bar{M}L^2}{2w^{\text{FEM}}(0)}, \quad (30)$$

where $w^{\text{FEM}}(0)$ is the deflection of the FEM solution averaged over the left edge ($x = 0$). Calculating the bending stiffness using Equations 25 or 30 ends with the same result which we tested numerically.

The effective material properties of the large specimens can be obtained by the standard computational periodic first-order homogenization produced by a unit cell with periodic boundary condition which is identified later as $\mathbb{C}_{\text{macro}}$ in Section 5.1. As we will show later the macro elasticity tensor $\mathbb{C}_{\text{macro}}$ is not isotropic and shows tetragonal symmetry. The size-effects are shown via the so-called normalized bending stiffness \bar{D}/D_{macro} plotted in Figure 5 which relates the actual stiffness of the fully discretized metamaterial to the one obtained from homogenized linear elasticity with $\mathbb{C}_{\text{macro}}$ which reads analytically

$$D_{\text{macro}} = \frac{E_{\text{macro}} H^3}{12(1 - \nu_{\text{macro}}^2)}. \quad (31)$$

The normalized bending stiffness approaches the value one when we increase the specimen size. Applying a rotation (loading case 1) or a moment (loading case 2) leads to similar results as expected.

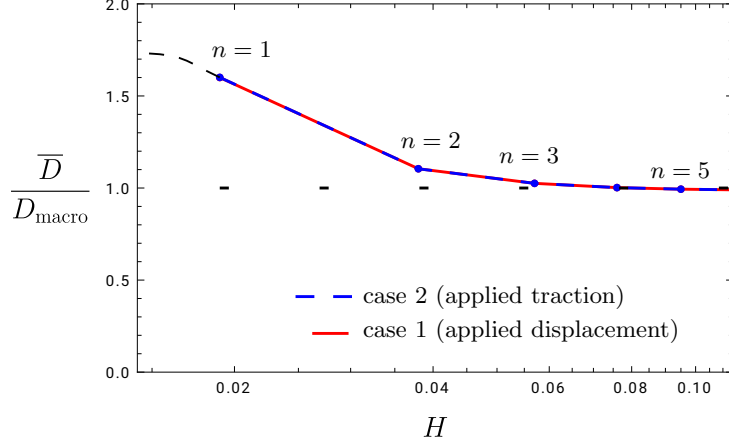


Figure 5: The normalized bending stiffness varying the beam size $H \times L = nl \times 12nl$. Note that the left blacked dashed line is a fictitious extrapolation, taking into account that the stiffness will remain finite.

5 Size-effects of the relaxed micromorphic continuum subjected to pure bending

The previous size-effects shown by the fully resolved heterogeneous material should be reproduced by the relaxed micromorphic model. However, the boundary conditions and material parameters identification are not obvious.

5.1 Identification of $\mathbb{C}_{\text{macro}}$

The macro elasticity tensor $\mathbb{C}_{\text{macro}}$ corresponds to the case $L_c \rightarrow 0$ equivalent to large values of n where the macro homogeneous response is expected. A unit cell with periodic boundary conditions should be used, see for example [104]. The geometry of the unit cell has no role for this standard analysis. Our analysis shows that $\mathbb{C}_{\text{macro}}$ has the tetragonal symmetry property for our assumed metamaterial and it reads in Voigt notation

$$\mathbb{C}_{\text{macro}} = \begin{pmatrix} 2\mu_{\text{macro}} + \lambda_{\text{macro}} & \lambda_{\text{macro}} & 0 \\ \lambda_{\text{macro}} & 2\mu_{\text{macro}} + \lambda_{\text{macro}} & 0 \\ 0 & 0 & \mu_{\text{macro}}^* \end{pmatrix}, \quad (32)$$

where three parameters need to be defined. We obtain by our numerical analysis

$$\mathbb{C}_{\text{macro}} = \begin{pmatrix} 47.86 & 17.61 & 0 \\ 17.61 & 47.86 & 0 \\ 0 & 0 & 9.98 \end{pmatrix} [\text{GPa}] \Rightarrow \begin{matrix} \lambda_{\text{macro}} & = & 17.61 & \text{GPa} \\ \mu_{\text{macro}} & = & 15.13 & \text{GPa} \\ \mu_{\text{macro}}^* & = & 9.98 & \text{GPa} \end{matrix}. \quad (33)$$

5.2 Identification of $\mathbb{C}_{\text{micro}}$ (first approach)

The micro elasticity tensor $\mathbb{C}_{\text{micro}}$ in the relaxed micromorphic model is defined as the maximum stiffness on the micro-scale which must have the tetragonal symmetry similar to $\mathbb{C}_{\text{macro}}$ according to the extended Neumann's principle [66]. The affine Dirichlet boundary conditions are the proper ones which preserve material symmetries. However, different variants of unit cells must be investigated for the affine Dirichlet boundary conditions. For each choice of a unit cell $i = 1, \dots, r$ with the affine Dirichlet boundary conditions, we obtain the corresponding apparent stiffness tensor denoted as \mathbb{C}_i^D . The positive definite micro elasticity tensor will be set as the least upper bound of the apparent stiffness of the microstructure measured in the energy norm following the Löwner matrix supremum problem, see for details [66].

For the assumed metamaterial, four different variants of the unit cell are valid, see Figure 6, which lead to the elasticity tensors $\mathbb{C}_i^D, i = 1, \dots, 4$ with the tetragonal symmetry property as intended. The results are summarized in Table 2.

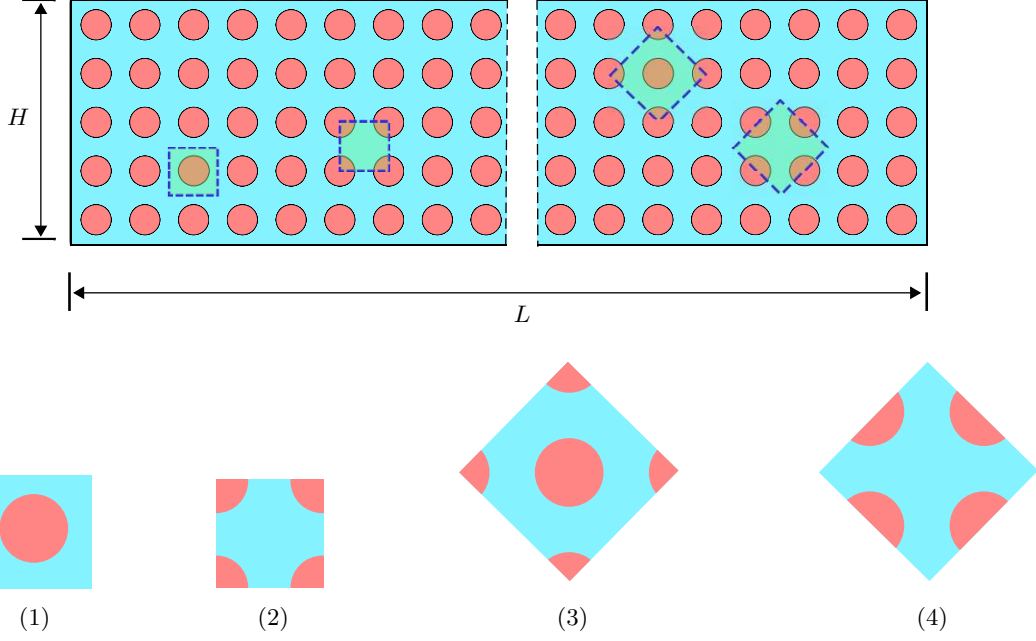


Figure 6: The possible choices of the unit cells with tetragonal symmetry. The edge length of the unit cell equals to l for (1) and (2) and $\sqrt{2}l$ for (3) and (4).

Table 2: The elasticity parameters of the unit cells in Figure 6 under affine Dirichlet boundary conditions. The elasticity parameters define elasticity tensors which exhibit tetragonal symmetry similar to $\mathbb{C}_{\text{macro}}$.

unit cell	λ_i [GPa]	μ_i [GPa]	μ_i^* [GPa]
1	18.26	15.34	14.61
2	20.15	15.83	14.44
3	19.25	15.54	13.19
4	19.56	15.66	12.68

The micro elasticity tensor $\mathbb{C}_{\text{micro}}^{\text{L\"owner}}$ is defined then by the L\"owner matrix supremum problem as

$$\tilde{\boldsymbol{\varepsilon}} : \mathbb{C}_{\text{micro}}^{\text{L\"owner}} : \tilde{\boldsymbol{\varepsilon}} \geq \tilde{\boldsymbol{\varepsilon}} : \mathbb{C}_i^{\text{D}} : \tilde{\boldsymbol{\varepsilon}} \quad \text{where } i=1,\dots,4 \quad , \quad \forall \tilde{\boldsymbol{\varepsilon}} \in \text{Sym}(3). \quad (34)$$

which turns for the tetragonal symmetry case to the following one written in Voigt notation

$$\begin{aligned} \begin{pmatrix} \tilde{\varepsilon}_{11} \\ \tilde{\varepsilon}_{22} \\ 2\tilde{\varepsilon}_{12} \end{pmatrix} : \begin{pmatrix} 2\mu_{\text{micro}}^{\text{L\"owner}} + \lambda_{\text{micro}}^{\text{L\"owner}} & \lambda_{\text{micro}}^{\text{L\"owner}} & 0 \\ \lambda_{\text{micro}}^{\text{L\"owner}} & 2\mu_{\text{micro}}^{\text{L\"owner}} + \lambda_{\text{micro}}^{\text{L\"owner}} & 0 \\ 0 & 0 & (\mu^*)_{\text{micro}}^{\text{L\"owner}} \end{pmatrix} : \begin{pmatrix} \tilde{\varepsilon}_{11} \\ \tilde{\varepsilon}_{22} \\ 2\tilde{\varepsilon}_{12} \end{pmatrix} \geq \\ \begin{pmatrix} \tilde{\varepsilon}_{11} \\ \tilde{\varepsilon}_{22} \\ 2\tilde{\varepsilon}_{12} \end{pmatrix} : \begin{pmatrix} 2\mu_i + \lambda_i & \lambda_i & 0 \\ \lambda_i & 2\mu_i + \lambda_i & 0 \\ 0 & 0 & \mu_i^* \end{pmatrix} : \begin{pmatrix} \tilde{\varepsilon}_{11} \\ \tilde{\varepsilon}_{22} \\ 2\tilde{\varepsilon}_{12} \end{pmatrix} \quad \text{for } i=1,\dots,4 \quad , \quad \forall \begin{pmatrix} \tilde{\varepsilon}_{11} \\ \tilde{\varepsilon}_{22} \\ \tilde{\varepsilon}_{12} \end{pmatrix} \in \mathbb{R}^3. \end{aligned} \quad (35)$$

The solution of the previous problem reads

$$(\mu^*)_{\text{micro}}^{\text{L\"owner}} \geq \max_i \{\mu_i^*\}, \quad \mu_{\text{micro}}^{\text{L\"owner}} \geq \max_i \{\mu_i\}, \quad \lambda_{\text{micro}}^{\text{L\"owner}} + \mu_{\text{micro}}^{\text{L\"owner}} \geq \max_i \{\mu_i + \lambda_i\}, \quad (36)$$

for $i = 1, \dots, 4$. We take therefore (see Table 2)

$$\begin{aligned} (\mu^*)_{\text{micro}}^{\text{L\"owner}} &:= \mu_1^* = 14.61 \text{ GPa}, \quad \mu_{\text{micro}}^{\text{L\"owner}} := \mu_2 = 15.83 \text{ GPa}, \\ \lambda_{\text{micro}}^{\text{L\"owner}} &:= \mu_2 + \lambda_2 - \mu_{\text{micro}} = 20.15 \text{ GPa}, \end{aligned} \quad (37)$$

and thus

$$\mathbb{C}_{\text{micro}}^{\text{L\"owner}} := \begin{pmatrix} 51.81 & 20.15 & 0 \\ 20.15 & 51.81 & 0 \\ 0 & 0 & 14.61 \end{pmatrix} [\text{GPa}]. \quad (38)$$

However, the previous estimate will serve as a lower bound for $\mathbb{C}_{\text{micro}}$. In Figure 7, we show the size-effect of the fully resolved metamaterial beams and the linear elasticity solutions with different elasticity tensors: I) $\mathbb{C}_{\text{macro}}$, II) $\mathbb{C}_{\text{micro}}^{\text{L\"owner}}$, III) $\mathbb{C}_{\text{matrix}}$ of the homogeneous isotropic matrix, and IV) $\mathbb{C}_{\text{Voigt}}$ which is isotropic and obtained by the equal strain assumption $\mathbb{C}_{\text{Voigt}} = \phi_{\text{matrix}}\mathbb{C}_{\text{matrix}} + \phi_{\text{inclusion}}\mathbb{C}_{\text{inclusion}}$ where ϕ_{matrix} and $\phi_{\text{inclusion}}$ are the volume fractions of the matrix and inclusion, respectively. The calculated value for $\mathbb{C}_{\text{micro}}^{\text{L\"owner}}$ is too soft compared to the micro-structured beams and even the linear elasticity with $\mathbb{C}_{\text{Voigt}}$ is softer than the solution of the fully resolved metamaterial beam for $n = 1$. This can be explained by the fact that the bending deformation mode is not captured by the affine Dirichlet boundary conditions. Therefore, we relate $\mathbb{C}_{\text{micro}}$ to the matrix stiffness $\mathbb{C}_{\text{matrix}}$ and introduce a scalar $\alpha \geq 1$ so that we have $\mathbb{C}_{\text{micro}} := \alpha \mathbb{C}_{\text{micro}}^{\text{L\"owner}}$. We define an upper limit for $\mathbb{C}_{\text{micro}}$ as

$$\tilde{\boldsymbol{\varepsilon}} : \mathbb{C}_{\text{matrix}} : \tilde{\boldsymbol{\varepsilon}} \geq \tilde{\boldsymbol{\varepsilon}} : \mathbb{C}_{\text{micro}} : \tilde{\boldsymbol{\varepsilon}} = \tilde{\boldsymbol{\varepsilon}} : \alpha \mathbb{C}_{\text{micro}}^{\text{L\"owner}} : \tilde{\boldsymbol{\varepsilon}}, \quad \forall \tilde{\boldsymbol{\varepsilon}} \in \text{Sym}(3). \quad (39)$$

By introducing Equation 39 we keep the anisotropic symmetry property of $\mathbb{C}_{\text{micro}}$. However, the elasticity tensor $\mathbb{C}_{\text{matrix}}$ is isotropic. We obtain then

$$\mu_{\text{matrix}}^* = \mu_{\text{matrix}} \geq \alpha (\mu_{\text{micro}}^*)^{\text{L\"owner}}, \quad \mu_{\text{matrix}} \geq \alpha \mu_{\text{micro}}^{\text{L\"owner}}, \quad \lambda_{\text{matrix}} + \mu_{\text{matrix}} \geq \alpha (\lambda_{\text{micro}}^{\text{L\"owner}} + \mu_{\text{micro}}^{\text{L\"owner}}), \quad (40)$$

which leads to

$$\alpha \in [1, \min(\frac{\mu_{\text{matrix}}^*}{(\mu_{\text{micro}}^*)^{\text{L\"owner}}}, \frac{\mu_{\text{matrix}}}{\mu_{\text{micro}}^{\text{L\"owner}}}, \frac{\mu_{\text{matrix}} + \lambda_{\text{matrix}}}{\mu_{\text{micro}}^{\text{L\"owner}} + \lambda_{\text{micro}}^{\text{L\"owner}}})] = [1, 1.66]. \quad (41)$$

Figure 7 shows that linear elasticity with $\mathbb{C}_{\text{micro}} = 1.66 \mathbb{C}_{\text{micro}}^{\text{L\"owner}}$ is stiffer than the fully resolved metamaterial for $n = 1$ and therefore it is a valid choice. However, assuming $\mathbb{C}_{\text{micro}} = \mathbb{C}_{\text{matrix}}$ does not break the extended Neumann's principle. We will investigate later numerically the consequences of the different choices for $\mathbb{C}_{\text{micro}}$.

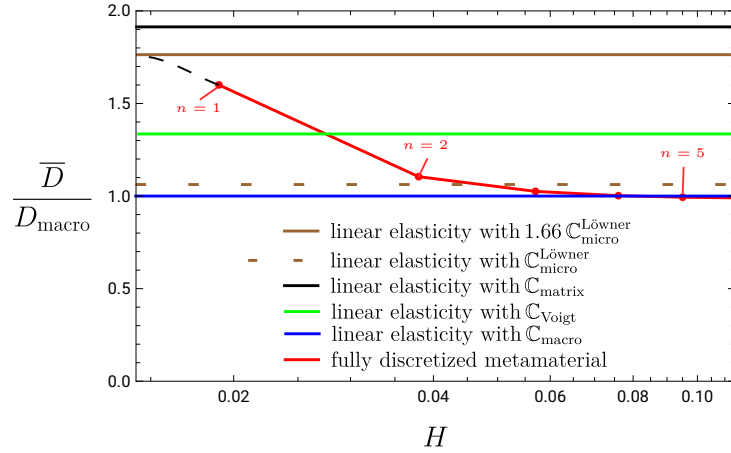


Figure 7: The normalized bending stiffness varying the the beam size $H \times L = nl \times 12nl$ compared to the ones obtained by linear elasticity with different elasticity tensors shown in Section 5.2.

5.3 Identification of $\mathbb{C}_{\text{micro}}$ (second approach)

We define in the following $\mathbb{C}_{\text{micro}}$ by scaling $\mathbb{C}_{\text{macro}}$ with a scalar $\beta > 1$, i.e.

$$\mathbb{C}_{\text{micro}} = \beta \mathbb{C}_{\text{macro}} \quad (42)$$

where β is defined as

$$\beta = \max(\frac{D_{\text{micro}}}{D_{\text{macro}}}). \quad (43)$$

Here, D_{micro} is the bending stiffness of any fully discretized unit cell or cluster of unit cells and D_{macro} is the bending stiffness of the standard linear elasticity with $\mathbb{C}_{\text{macro}}$ for a domain with the same dimensions. Figure 8 shows exemplarily the procedure for one single unit cell.

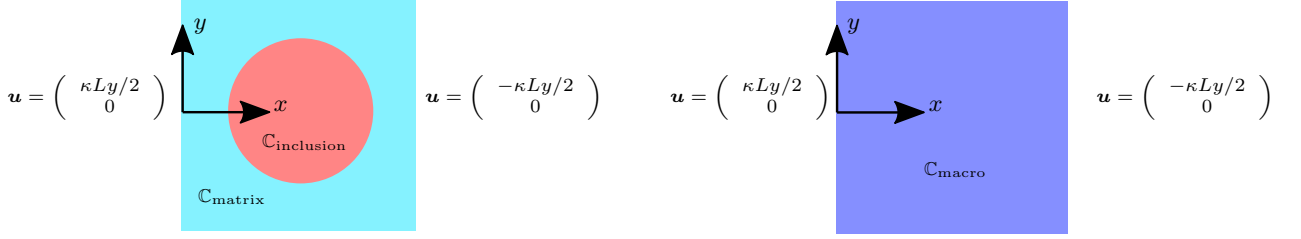


Figure 8: Illustration shows the calculations of D_{micro} (left) and D_{macro} (right) used to calculate β .

We investigate the stiffest response which can be obtained, i.e. a biggest value of β . Our candidates with the possible stiffest response are shown in Figure 9. The candidates are based on one single unit cell with an inclusion on its center (type 1) or two half-inclusions on the left and right edges (type 2). Then, we add more unit cells in the height direction to investigate if the deep beam effect could exhibit even stiffer response.

The boundary value problem is built by rotating left and right edges for both the fully discretized microstructure and the homogeneous material with standard linear elasticity with $\mathbb{C}_{\text{macro}}$, see Figure 8. The computation of the bending stiffness can be based on an effective curvature $\bar{\kappa}$ similar to Section 4. Therefore, we define an effective deflection as

$$\bar{w}(x) = \frac{\bar{\kappa}}{2}(x^2 - lx) \quad \text{satisfying} \quad \bar{w}(0) = 0, \quad \text{and} \quad \bar{w}(l) = 0, \quad (44)$$

where the effective curvature is obtained by the least square minimization in Equation 28 as

$$\bar{\kappa} = \frac{\sum_I^{n_{\text{node}}} (d_I^y)_2 \frac{(\mathbf{X}_I)_1^2 - l(\mathbf{X}_I)_1}{2}}{\sum_I^{n_{\text{node}}} \left(\frac{(\mathbf{X}_I)_1^2 - l(\mathbf{X}_I)_1}{2} \right)^2}, \quad (45)$$

with \mathbf{X}_I and d_I^y as the coordinates and the displacement degrees of freedom at node I . The bending stiffness can be computed following Equation 26 as

$$D^1 = \frac{\bar{M}}{\bar{\kappa}}, \quad (46)$$

where \bar{M} is the moment calculated on the left or right edges by nodes reactions. Alternatively, the bending stiffness can be defined by using the deflection at the center $w^{\text{FEM}}(l/2)$ obtained via the FEM solution averaged over the height. Thus, we obtain

$$D^2 = -\frac{\bar{M}l^2}{8w^{\text{FEM}}(l/2)}. \quad (47)$$

We notice that the bending stiffness calculated by the effective curvature in Equation 46 is less than the one obtained by the deflection at the center in Equation 47. The explanation is that the deflection of the micro-structured metamaterial at the center is less than the effective one (in absolute values), which causes this difference. This is shown in Figure 10, where we show exemplarily the effective deflection \bar{w} and the deflection of the heterogeneous metamaterial w^{FEM} for the case $2l \times l$ of first and second type specimens. The deflection w^{FEM} is obtained from the FEM solution of the fully resolved microstructure by averaging the y -displacement over the height at each position x .

We summarize the results in Table 3 and choose $\beta = 1.98$. This choice guarantees that a homogeneous continuum with elasticity tensor $\mathbb{C}_{\text{micro}} = 1.98 \mathbb{C}_{\text{macro}}$ is always stiffer than the fully discretized metamaterial. In Figure 11, we show the size-effect of the fully resolved metamaterial beams and the linear elasticity solutions with elasticity tensors $\mathbb{C}_{\text{micro}} = 1.98 \mathbb{C}_{\text{macro}}$ and $\mathbb{C}_{\text{macro}}$. The upper limit $\mathbb{C}_{\text{micro}} = 1.98 \mathbb{C}_{\text{macro}}$ is stiffer than the relatively stiffest metamaterial beam ($n = 1$) which confirms its validity.

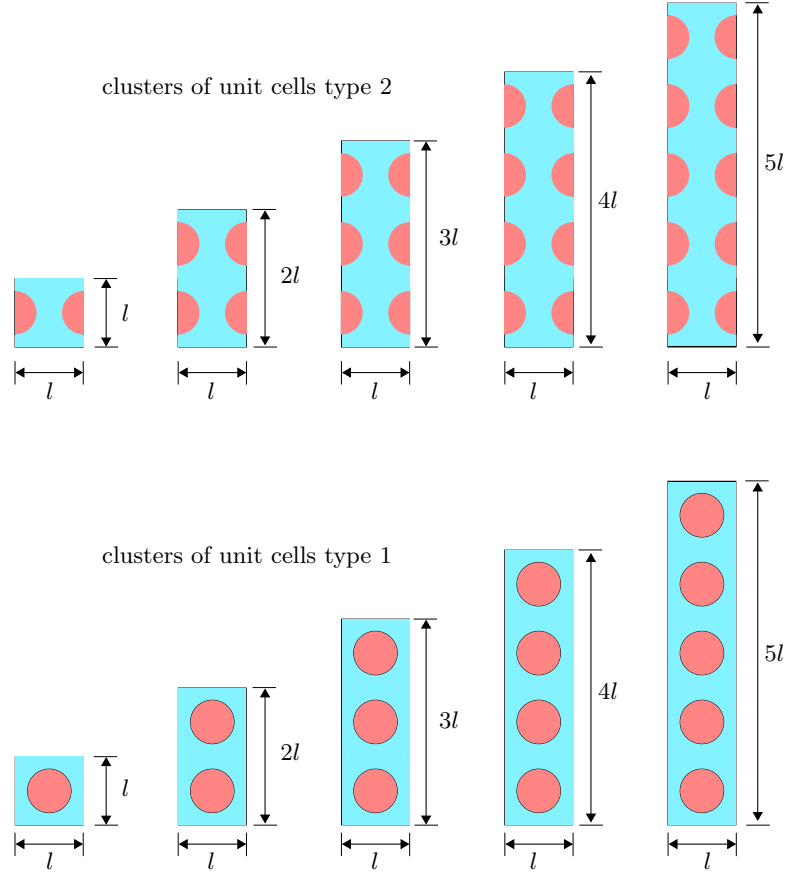


Figure 9: Illustration shows the possible candidates with largest normalized bending stiffness.

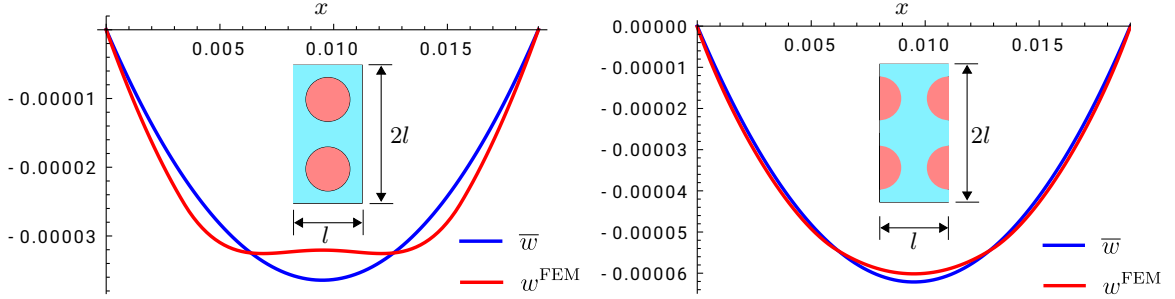


Figure 10: The deflection curves \bar{w} and w^{FEM} for the case $2l \times l$ of first type (left) and second type (right) specimens shown in Figure 9. \bar{w} is the effective deflection defined in Equation 44 while w^{FEM} is the deflection of the FEM solution of the fully resolved microstructure obtained by averaging the displacement in y -direction over the height at each position x . The effective deflection at $x = l/2$ is larger than the deflection of the heterogeneous solution at $x = l/2$ (in absolute values) and therefore the bending stiffness obtained by Equation 47 is larger than the one calculated by Equation 46, see Table 3.

5.4 Identification of \mathbb{C}_e

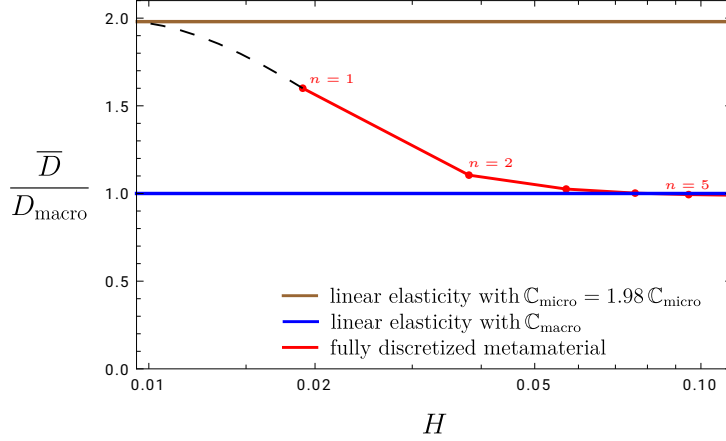
The elasticity tensor \mathbb{C}_e is calculated via the micro-macro Reuss-like homogenization formula

$$\mathbb{C}_{\text{macro}}^{-1} = \mathbb{C}_{\text{micro}}^{-1} + \mathbb{C}_e^{-1} \quad \Rightarrow \quad \mathbb{C}_e = \mathbb{C}_{\text{micro}}(\mathbb{C}_{\text{micro}} - \mathbb{C}_{\text{macro}})^{-1}\mathbb{C}_{\text{macro}}. \quad (48)$$

The obtained elasticity tensor \mathbb{C}_e is automatically positive definite since $\mathbb{C}_{\text{micro}} > \mathbb{C}_{\text{macro}}$ and has tetragonal symmetry property. However, no obvious physical interpretation can be assigned to the tensor \mathbb{C}_e .

Table 3: The results of the analysis illustrated in Figure 8 for the specimens which are shown in Figure 9.

$H \times L$	Type 1		Type 2	
	$\frac{D_{\text{micro}}^1}{D_{\text{macro}}^1}$	$\frac{D_{\text{micro}}^2}{D_{\text{macro}}^2}$	$\frac{D_{\text{micro}}^1}{D_{\text{macro}}^1}$	$\frac{D_{\text{micro}}^2}{D_{\text{macro}}^2}$
$l \times l$	1.81	1.98	1.07	1.11
$2l \times l$	1.29	1.47	0.82	0.84
$3l \times l$	1.23	1.43	0.77	0.8
$4l \times l$	1.22	1.43	0.76	0.78
$5l \times l$	1.21	1.43	0.75	0.78

Figure 11: The normalized bending stiffness varying the the beam size $H \times L = nl \times 12nl$ compared to the ones obtained by linear elasticity with different elasticity tensors shown in Section 5.3.

5.5 The boundary conditions of the micro-distortion field

The boundary conditions (BCs) of the micro-distortion field are key components for the relaxed micromorphic model. The boundary conditions should be chosen in a way that induces a curvature in the model, i.e. $\text{Curl } \mathbf{P} \neq \mathbf{0}$. Otherwise, insufficient boundary condition of the microdistortion field can cause pathological behavior of the relaxed micromorphic model. This behavior is represented by showing no size-effects or not reaching the intended upper limit (linear elasticity with $\mathbb{C}_{\text{micro}}$) for $L_c \rightarrow \infty$.

5.5.1 Symmetric force stress case:

We assume here $\mathbb{C}_c = 0$ which causes symmetric force stress $\boldsymbol{\sigma}$ and symmetric $\text{Curl } \mathbf{m}$ because Equation 9d becomes symmetric. We test the sufficiency of the boundary condition by comparing the solution of the relaxed micromorphic model for varied values of the characteristic length with the solutions obtained by the standard linear elasticity with elasticity tensors $\mathbb{C}_{\text{micro}}$ and $\mathbb{C}_{\text{macro}}$. More specifically, the relaxed micromorphic model should reproduce linear elasticity with elasticity tensors $\mathbb{C}_{\text{micro}}$ and $\mathbb{C}_{\text{macro}}$ for $L_c \rightarrow \infty$ and $L_c \rightarrow 0$, respectively, see [21, 70–72, 74, 84].

We design a test by fixing the geometry $H \times L = 2l \times 24l$ with assuming $\mathbb{C}_{\text{micro}} = 1.98 \mathbb{C}_{\text{macro}}$ and setting $\mu = \mu_{\text{macro}}$. The boundary conditions of the displacement field are taken similar to the ones applied on the fully resolved metamaterials in Figure 3. For the first case with applied rotation, the consistent coupling condition can be applied completely on the right edge and partially on the left edge, see Figure 12. Indeed, applying the consistent coupling condition on the Dirichlet boundary of the displacement field is adequate to fulfill the theoretical limits of the relaxed micromorphic model. Removing the consistent coupling condition on left or right edges leads to vanishing curvature and turns the relaxed micromorphic model into standard linear elasticity with $\mathbb{C}_{\text{macro}}$. The previous behavior is demonstrated in Figure 13. The exact same behavior is observed for the second loading case with applied traction if we apply the consistent coupling condition on the boundary corresponding to the first loading case, see Figure 12. However, the consistent coupling condition cannot be imposed explicitly on the right edge where the

linear traction is applied (the tangential components of the displacement gradient are not known) and therefore we enforce it via a penalty approach. Consequently, the relaxed micromorphic model results in consistent results for both loading cases, see Figure 13.

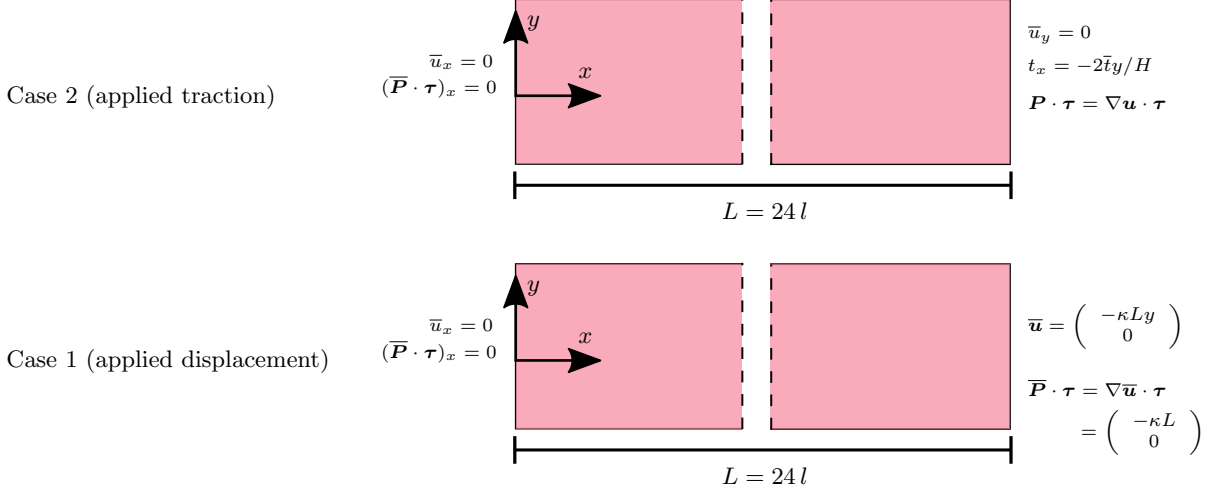


Figure 12: The boundary value problems of the homogeneous relaxed micromorphic model for both loading cases. These boundary value problems are equivalent to the two cases of the heterogeneous metamaterial shown in Figure 3. The upper and lower edges are traction-free. The consistent coupling condition is enforced at $x = L$ for the second case through penalty approach.

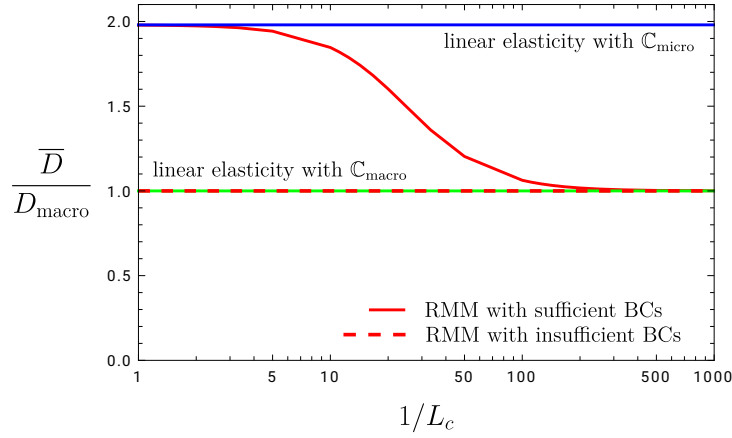
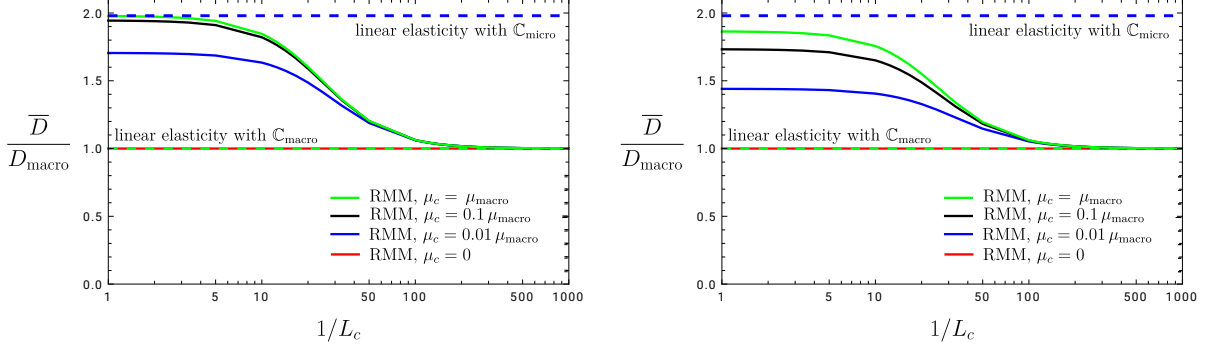


Figure 13: The normalized bending stiffness obtained by the relaxed micromorphic model for both loading cases assuming $\mathbb{C}_c = \mathbf{0}$ ($\mu_c = 0$) with varying the characteristic length L_c . Sufficient BCs indicate to apply the consistent coupling condition on the left and right edges, see Figure 12. Removing the consistent coupling condition on left or right edge is considered as insufficient and leads to no size-effect.

5.5.2 Non-symmetric force stress case: Here, we assume $\mathbb{C}_c = 2\mu_c \mathbb{I}$ where \mathbb{I} is the fourth order identity tensor and μ_c is the Cosserat couple modulus. We study the influence of varying the Cosserat couple modulus $\mu_c \in [0, 0.01, 0.1, 1] * \mu_{\text{macro}}$ considering different scenarios of the boundary condition of \mathbf{P} . The geometry and the remaining material parameters are taken as for the symmetric case, see Section 5.5.1.

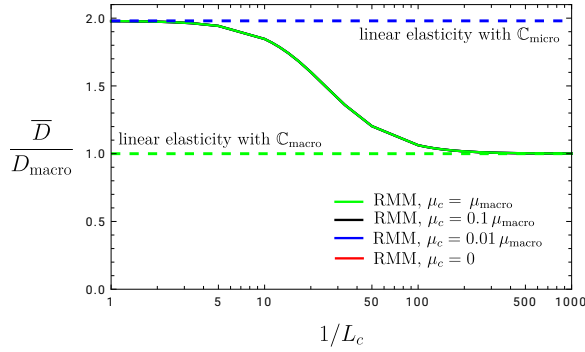
In Figure 14, we show the normalized bending stiffness for the cases a) the consistent coupling condition is applied partially on the left edge, b) the consistent coupling condition is applied fully on the right edge only, and c) the consistent coupling condition is applied partially on the left edge and fully on the right edge. Size-effects are noticed even if the consistent coupling condition is not placed on the right and left

edges simultaneously which is not the case for the symmetric force case ($\mu_c = 0$). Increasing the Cosserat couple modulus μ_c raises the stiffness of the relaxed micromorphic model closer to linear elasticity with $\mathbb{C}_{\text{micro}}$ for $L_c \rightarrow \infty$ and even reach it in Figure 14(a). However, it is not guaranteed that the relaxed micromorphic model achieves linear elasticity with $\mathbb{C}_{\text{micro}}$ for $L_c \rightarrow \infty$, see Figure 14(b). The results of enforcing the consistent coupling condition on both left and right edges are equivalent for the symmetric and non-symmetric cases in Figures 13 and 14(c), respectively, and the Cosserat couple modulus has no influence.



(a) consistent coupling condition on the left edge only

(b) consistent coupling condition on the right edge only



(c) consistent coupling condition on the left and right edges

Figure 14: The normalized bending stiffness obtained by the relaxed micromorphic model for both loading cases with non-symmetric force stress and with varying the characteristic length L_c . Different scenarios are investigated for the boundary conditions of the micro-distortion field.

5.5.3 Special case of a skew-symmetric micro-distortion field: For the case of $\mathbb{C}_{\text{micro}} \rightarrow \infty$, the micro-distortion field \mathbf{P} must be skew-symmetric and the Cosserat model is recovered, c.f. [10, 17, 33, 44]. We investigate here the influence of enforcing the consistent coupling condition on the left, right and both left and right edges for $\mathbb{C}_{\text{micro}} = 1000 \mathbb{C}_{\text{macro}}$. Different values of the Cosserat couple modulus μ_c are assumed for varied values of the characteristic length L_c in Figure 15. We notice that linear elasticity with elasticity tensor $\mathbb{C}_{\text{micro}}$ is recognized as an upper limit only when the consistent coupling condition is enforced on both left and right edges in Figure 15(c). Weak size-effects are noticed, i.e. $\frac{\bar{D}}{D_{\text{macro}}} \ll \frac{D_{\text{micro}}}{D_{\text{macro}}}$, when the consistent coupling condition is set only on the right edge, Figure 15(b). Unbounded stiffness can be observed when the consistent coupling condition is enforced partially on the left edge, see Figure 15(a). While size-effects are prompted only for non-vanishing Cosserat couple modulus $\mu_c \neq 0$ when the consistent coupling condition is applied either on left or right edges, enforcing the consistent coupling condition on both left and right edges simultaneously allows the model to act on the intended theoretical range with no influence of the Cosserat couple modulus μ_c . This can be explained that the skew-symmetric part of the micro-distortion field is same as the skew-symmetric part of the gradient of the displacement, see [71], which is the case in Figures 14(c) and 15(c).

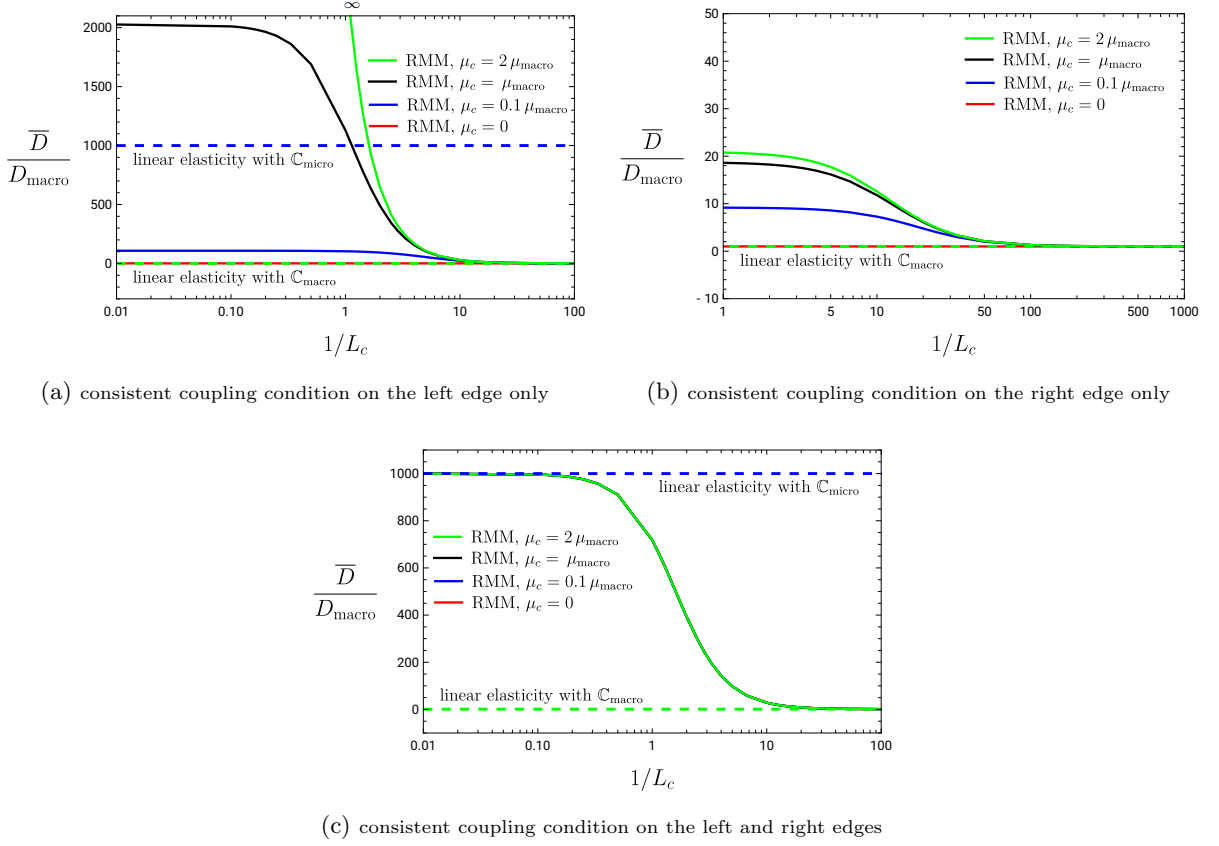


Figure 15: The normalized bending stiffness obtained by the relaxed micromorphic model for both loading cases with non-symmetric force stress and with varying the characteristic length L_c . Here, we assume $\mathbb{C}_{\text{micro}} = 1000\mathbb{C}_{\text{macro}}$ leading to a skew-symmetric micro-distortion field which retrieves the Cosserat model since the curvature expression is then equivalent with the Cosserat framework, see [33]. Different scenarios are investigated for the boundary conditions of the micro-distortion field.

5.6 Scaling of the curvature

The curvature for the 2D case is isotropic because $\text{Curl } \mathbf{P}$ is reduced to a vector. Therefore, the curvature will be controlled by only one parameter with assuming $\mathbb{L} = \mathbb{I}$ is the fourth order identity tensor. Since the parameters μ and L_c should be set constant independent of the specimen size, the curvature is modified by incorporating the size of the beams through the number n . Figure 5 shows that stiffer response is observed for smaller values of the number n ($n = 1$ is the stiffest). The relaxed micromorphic model exhibits stiffer response for bigger values of the characteristic length L_c (inversely proportional to n), see for example Figure 13. Therefore, we scale L_c by dividing by n and the curvature is modified to

$$\frac{1}{2}\mu L_c^2 \text{Curl } \mathbf{P} : \mathbb{L} : \text{Curl } \mathbf{P} \quad \Rightarrow \quad \frac{1}{2}\mu \left(\frac{L_c}{n}\right)^2 \text{Curl } \mathbf{P} : \text{Curl } \mathbf{P}. \quad (49)$$

Hence, for a constant L_c smaller values are obtained for the term L_c/n by increasing the beam size (increasing n) which reproduces the intended size-effects (smaller is stiffer). This modification of L_c is not ad hoc, but follows from a rigorous scaling argument, c.f. [66].

6 Final calibration

Now, we provide an identification scheme for the scale-independent material parameters of the relaxed micromorphic model. The boundary conditions of the micro-distortion field are determined in order to guarantee the intended behavior of the relaxed micromorphic model and the influence of the characteristic length L_c for both loading cases. For this calibration we assume symmetric force stress, i.e. $\mathbb{C}_c = \mathbf{0}$. As we

discussed in Sections 5.2, 5.3 and 5.5.3, different choices can be made for $\mathbb{C}_{\text{micro}}$, e.g. $\mathbb{C}_{\text{micro}} = 1.66 \mathbb{C}_{\text{micro}}^{\text{Löwner}}$, $\mathbb{C}_{\text{micro}} = \mathbb{C}_{\text{matrix}}$, $\mathbb{C}_{\text{micro}} = 1.98 \mathbb{C}_{\text{macro}}$ and $\mathbb{C}_{\text{micro}} = 1000 \mathbb{C}_{\text{macro}}$. For each choice of $\mathbb{C}_{\text{micro}}$, the curvature should be calibrated by means of L_c and μ . It is always possible to assume the shear modulus $\mu = \mu_{\text{macro}}$ and then the characteristic length L_c should be selected by fitting the fully detailed metamaterial, Figure 16. Alternatively, the characteristic length L_c can be set in advance, e.g. $L_c = l$, and then the shear modulus μ should fit the fully discretized metamaterial, see Figure 17 and Equation 49. We observe that increasing $\mathbb{C}_{\text{micro}}$ drastically leading to a ‘‘Cosserat’’ model interferes with the identification of the curvature terms and therefore a good fit can not be achieved, i.e. the metamaterial beam is not a Cosserat material.

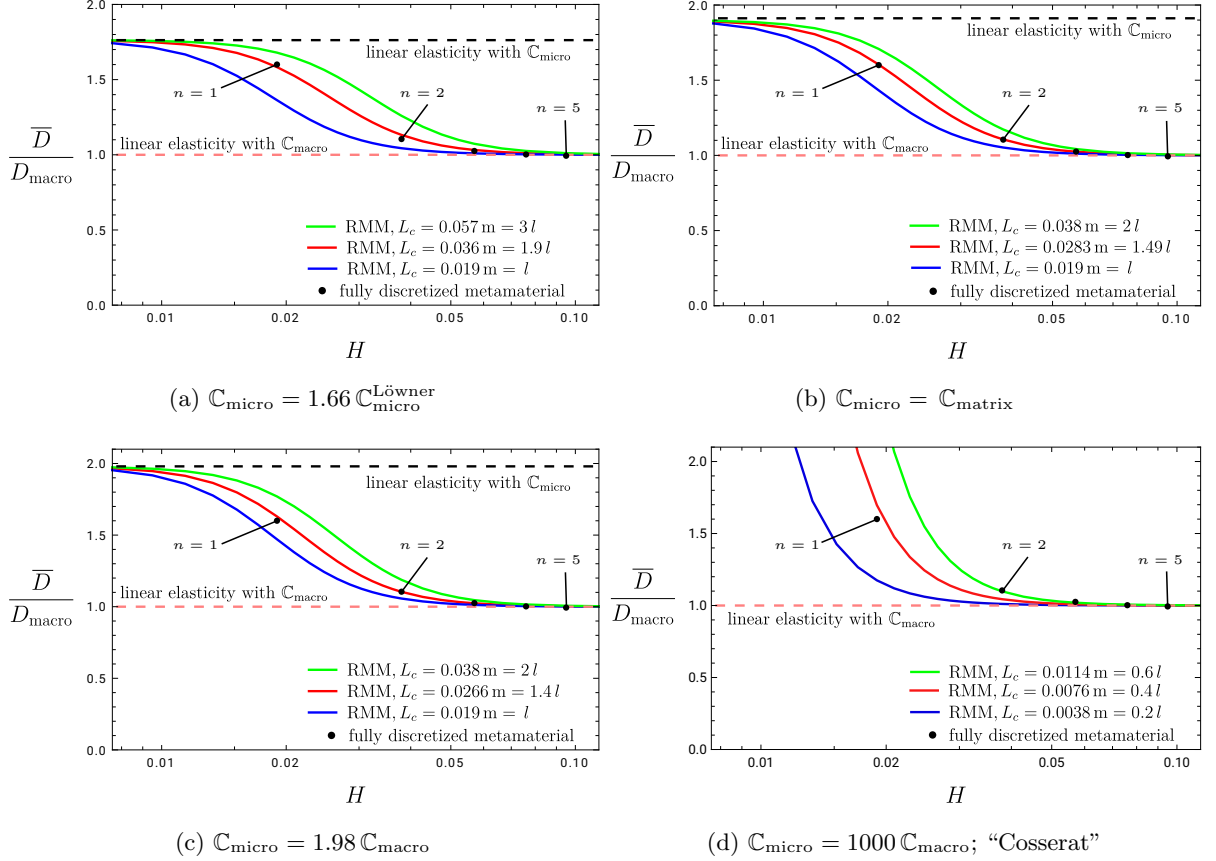


Figure 16: The normalized bending stiffness varying the beam size $H \times L = n l \times 12 n l$ obtained by the fully discretized metamaterial and the relaxed micromorphic model. We analyze here different choices for $\mathbb{C}_{\text{micro}}$ with varying L_c and fixing $\mu = \mu_{\text{macro}}$. The results are equivalent for both loading cases. ‘‘Cosserat’’ ($\mathbb{C}_{\text{micro}} = 1000 \mathbb{C}_{\text{macro}}$) can not provide a good fit.

7 Conclusions

We introduced the relaxed micromorphic model with a brief description of the suitable tangential-conforming finite element formulation. We studied the size-effect phenomena of fully resolved beams under bending. We have shown that applying a rotation (via a given displacement) or moment (applied traction) on the fully discretized metamaterial leads to similar results which we should get as well when we use the relaxed micromorphic model. We defined the macro elasticity tensor $\mathbb{C}_{\text{macro}}$ by means of the standard periodic homogenization corresponding to large specimens. The micro elasticity tensor is connected to the stiffest possible response of the assumed metamaterial. We introduced an approach to defining $\mathbb{C}_{\text{micro}}$ which is based on the least upper bound of the apparent stiffness of the microstructure measured in the energy norm following the Löwner matrix supremum problem where different variants of unit cells are considered under the affine Dirichlet boundary conditions. However, the flexural deformation mode is not captured by affine Dirichlet boundary conditions and the resulting elasticity tensor

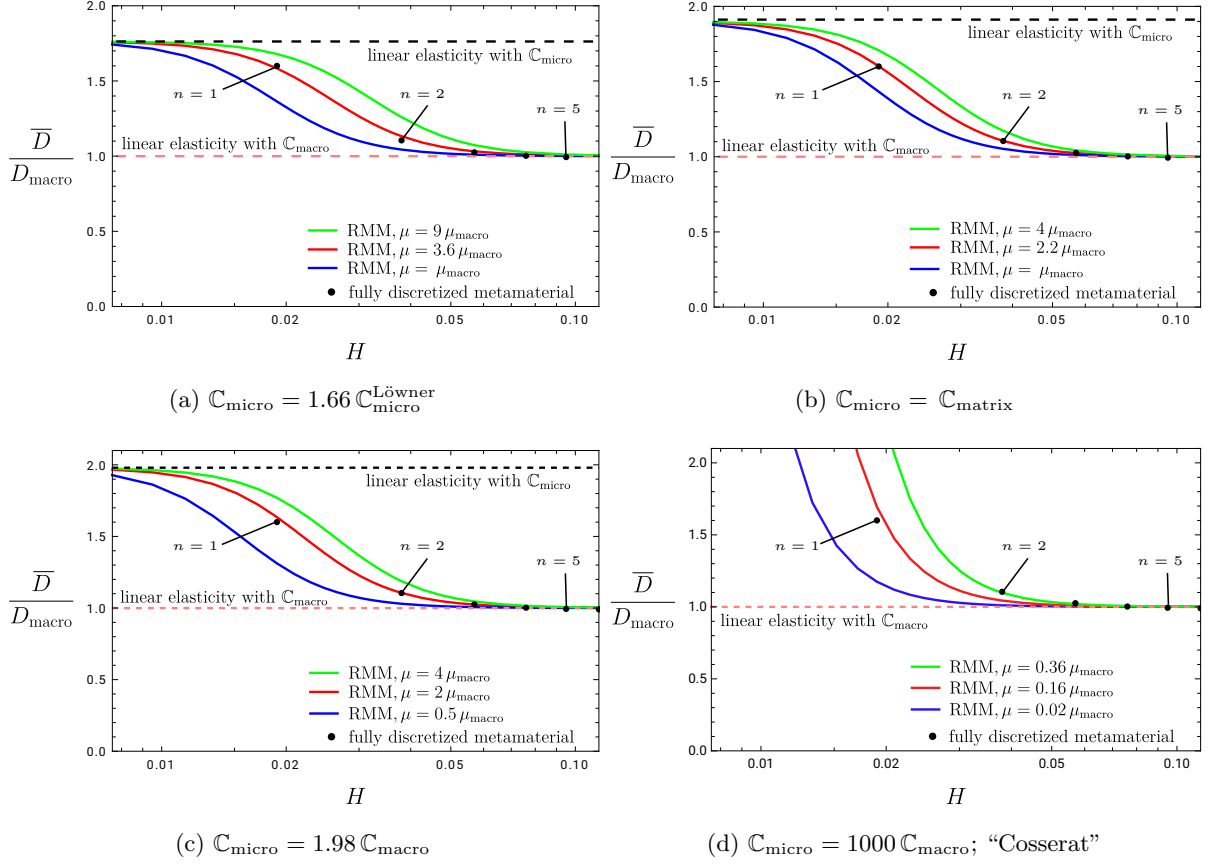


Figure 17: The normalized bending stiffness varying the beam size $H \times L = nl \times 12nl$ obtained by the fully discretized metamaterial and the relaxed micromorphic model. We analyze here different choices for $\mathbb{C}_{\text{micro}}$ with varying μ and fixing $L_c = l$. The results are equivalent for both loading cases. "Cosserat" ($\mathbb{C}_{\text{micro}} = 1000 \mathbb{C}_{\text{macro}}$) can not provide a good fit.

is much softer than the bent fully resolved metamaterial beams. Therefore, we scaled up the resulting elasticity tensor keeping its anisotropic tetragonal symmetry. Another procedure is tested to identify the micro elasticity tensor by non-affine boundary conditions (bending) on the unit cell or cluster of unit cells with the possible largest flexural rigidity. The boundary conditions were investigated for both loading cases (rotation or moment) for the symmetric and non-symmetric force stress. The consistent coupling boundary condition permits the model to work on the whole intended range bounded by linear elasticity with micro and macro elasticity tensors from above and below, respectively. Finally, we scaled the curvature measurement, which is isotropic in 2D, to account for the beam's size where a final fitting is conducted to decide the values of characteristic length and the shear modulus associated with the Curl of the micro-distortion field. The relaxed micromorphic delivers successfully the size-effects in a consistent manner for both loading cases.

Acknowledgment

Funded by the Deutsche Forschungsgemeinschaft (DFG, German research Foundation) - Project number 440935806 (SCHR 570/39-1, SCHE 2134/1-1, NE 902/10-1) within the DFG priority program 2256.

References

- [1] B. E. Abali. Revealing the physical insight of a length-scale parameter in metamaterials by exploiting the variational formulation. *Continuum Mechanics and Thermodynamics*, 31:885–894, 2019.
- [2] B. E. Abali and E. Barchiesi. Additive manufacturing introduced substructure and computational determination of

- metamaterials parameters by means of the asymptotic homogenization. *Continuum Mechanics and Thermodynamics*, 33:993–1009, 2021.
- [3] B. E. Abali, H. Yang, and P. Papadopoulos. A computational approach for determination of parameters in generalized mechanics. In H. Altenbach, W. H. Müller, and B. E. Abali, editors, *Higher Gradient Materials and Related Generalized Continua*, pages 1–18. Springer International Publishing, Cham, 2019.
- [4] B. E. Abali, B. Vazic, and P. Newell. Influence of microstructure on size effect for metamaterials applied in composite structures. *Mechanics Research Communications*, 122:103877, 2022.
- [5] E. C. Aifantis. On the gradient approach - Relation to Eringen’s nonlocal theory. *International Journal of Engineering Science*, 49(12):1367–1377, 2011.
- [6] A. Aivaliotis, D. Tallarico, M. V. d’Agostino, A. Daouadji, P. Neff, and A. Madeo. Frequency- and angle-dependent scattering of a finite-sized meta-structure via the relaxed micromorphic model. *Archive of Applied Mechanics*, 90: 1073–1096, 2020.
- [7] K. S. Al-Basyouni, A. Tounsi, and S. R. Mahmoud. Size dependent bending and vibration analysis of functionally graded micro beams based on modified couple stress theory and neutral surface position. *Composite Structures*, 125: 621–630, 2015.
- [8] S. E. Alavi, J.-F. Ganghoffer, H. Reda, and M. Sadighi. Construction of micromorphic continua by homogenization based on variational principles. *Journal of the Mechanics and Physics of Solids*, 153:104278, 2021.
- [9] S. E. Alavi, J.-F. Ganghoffer, and M. Sadighi. Chiral Cosserat homogenized constitutive models of architected media based on micromorphic homogenization. *Mathematics and Mechanics of Solids*, 27(10):2287–2313, 2022.
- [10] S.E. Alavi, J.F. Ganghoffer, M. Sadighi, M. Nasimsobhan, and A.H. Akbarzadeh. Continualization method of lattice materials and analysis of size effects revisited based on cosserat models. *International Journal of Solids and Structures*, 254-255:111894, 2022.
- [11] B. S. Altan and E. C. Aifantis. On some aspects in the special theory of gradient elasticity. *Journal of the Mechanical Behavior of Materials*, 8(3):231–282, 1997.
- [12] H. Askes and E. C. Aifantis. Gradient elasticity in statics and dynamics: An overview of formulations, length scale identification procedures, finite element implementations and new results. *International Journal of Solids and Structures*, 48(13):1962–1990, 2011.
- [13] H. Askes, A. V. Metrikine, A. V. Pichugin, and T. Bennett. Four simplified gradient elasticity models for the simulation of dispersive wave propagation. *Philosophical Magazine*, 88(28-29):3415–3443, 2008.
- [14] A. Bacigalupo, M. Paggi, F. Dal Corso, and D. Bigoni. Identification of higher-order continua equivalent to a Cauchy elastic composite. *Mechanics Research Communications*, 93:11–22, 2018. Mechanics from the 20th to the 21st Century: The Legacy of Gérard A. Maugin.
- [15] G. Barbagallo, D. Tallarico, M. V. d’Agostino, A. Aivaliotis, P. Neff, and A. Madeo. Relaxed micromorphic model of transient wave propagation in anisotropic band-gap metastructures. *International Journal of Solids and Structures*, 162:148–163, 2019.
- [16] R. Biswas and L. H. Poh. A micromorphic computational homogenization framework for heterogeneous materials. *Journal of the Mechanics and Physics of Solids*, 102:187–208, 2017.
- [17] T. Blesgen and P. Neff. Simple shear in nonlinear cosserat micropolar elasticity: Existence of minimizers, numerical simulations, and occurrence of microstructure. *Mathematics and Mechanics of Solids*, page 10812865221122191, 2022.
- [18] A. Carcaterra, F. dell’Isola, R. Esposito, and M. Pulvirenti. Macroscopic description of microscopically strongly inhomogeneous systems: A mathematical basis for the synthesis of higher gradients metamaterials. *Archive for Rational Mechanics and Analysis*, 218:1239–1262, 2015.
- [19] E. Cosserat and F. Cosserat. *Théorie des corps déformable*. Librairie Scientifique A. Hermann et Fils, engl. translation by D. H. Delphenich, pdf available at (<http://www.mathematik.tu-darmstadt.de/fbereiche/analysis/pde/staff/neff/patrizio/Cosserat.html>), reprint 2009 by Hermann Librairie Scientifique, ISBN 978 27056 6920 1, Paris, 1909.
- [20] M. V. d’Agostino, G. Barbagallo, I.-D. Ghiba, B. Eidel, P. Neff, and A. Madeo. Effective description of anisotropic wave dispersion in mechanical band-gap metamaterials via the relaxed micromorphic model. *Journal of Elasticity*, 139:299–329, 2020.
- [21] M. V. d’Agostino, G. Rizzi, H. Khan, P. Lewintan, A. Madeo, and P. Neff. The consistent coupling boundary condition for the classical micromorphic model: existence, uniqueness and interpretation of the parameters. *Continuum Mechanics and Thermodynamics*, 2022. doi: 10.1007/s00161-022-01126-3.
- [22] D. Del Vescovo and I. Giorgio. Dynamic problems for metamaterials: Review of existing models and ideas for further research. *International Journal of Engineering Science*, 80:153–172, 2014.
- [23] F. Demore, G. Rizzi, M. Collet, P. Neff, and A. Madeo. Unfolding engineering metamaterials design: Relaxed micromorphic modeling of large-scale acoustic meta-structures. *Journal of the Mechanics and Physics of Solids*, 168: 104995, 2022.
- [24] A. R. El Dhaba. Reduced micromorphic model in orthogonal curvilinear coordinates and its application to a meta-material hemisphere. *Scientific Reports*, 10, 2020.
- [25] V. A. Eremeyev, A. Cazzani, and F. dell’Isola. On nonlinear dilatational strain gradient elasticity. *Continuum Mechanics and Thermodynamics*, 33:1429–1463, 2021.

-
- [26] A. C. Eringen. Mechanics of micromorphic continua. In *Mechanics of Generalized Continua*, pages 18–35. Springer, Berlin, Heidelberg, 1968.
- [27] A. C. Eringen and E. S. Suhubi. Nonlinear theory of simple micro-elastic solids-I. *International Journal of Engineering Science*, 2(2):189–203, 1964.
- [28] P. Fischer, M. Klassen, J. Mergheim, P. Steinmann, and R. Müller. Isogeometric analysis of 2D gradient elasticity. *Computational Mechanics*, 47:1432–0924, 2011.
- [29] S. C. L. Fischer, L. Hillen, and C. Eberl. Mechanical metamaterials on the way from laboratory scale to industrial applications: Challenges for characterization and scalability. *Materials*, 13(16), 2020.
- [30] S. Forest. Homogenization methods and mechanics of generalized continua - part 2. *Theoretical and Applied Mechanics*, 28-29:113–144, 2002.
- [31] S. Forest and K. Sab. Cosserat overall modeling of heterogeneous materials. *Mechanics Research Communications*, 25(4):449–454, 1998.
- [32] I.-D. Ghiba, P. Neff, A. Madeo, L. Placidi, and G. Rosi. The relaxed linear micromorphic continuum: existence, uniqueness and continuous dependence in dynamics. *Mathematics and Mechanics of Solids*, 20(10):1171–1197, 2015.
- [33] I.-D. Ghiba, G. Rizzi, A. Madeo, and P. Neff. Cosserat micropolar elasticity: classical Eringen vs. dislocation form, 2022. URL <https://arxiv.org/abs/2206.02473>.
- [34] R. N. Glaesener, J.-H. Bastek, F. Gonon, V. Kannan, B. Telgen, B. Spöttling, S. Steiner, and D. M. Kochmann. Viscoelastic truss metamaterials as time-dependent generalized continua. *Journal of the Mechanics and Physics of Solids*, 156:104569, 2021.
- [35] I. Goda and J.-F. Ganghoffer. Construction of first and second order grade anisotropic continuum media for 3D porous and textile composite structures. *Composite Structures*, 141:292–327, 2016.
- [36] M. Golaszewski, R. Grygoruk, I. Giorgio, M. Laudato, and F. D. Cosmo. Metamaterials with relative displacements in their microstructure: technological challenges in 3d printing, experiments and numerical predictions. *Continuum Mechanics and Thermodynamics*, 31:1015–1034, 2019.
- [37] S. B. Hosseini and J. Niiranen. 3D strain gradient elasticity: Variational formulations, isogeometric analysis and model peculiarities. *Computer Methods in Applied Mechanics and Engineering*, 389:114324, 2022.
- [38] G. Hütter. Homogenization of a Cauchy continuum towards a micromorphic continuum. *Journal of the Mechanics and Physics of Solids*, 99:394–408, 2017.
- [39] G. Hütter. On the micro-macro relation for the microdeformation in the homogenization towards micromorphic and micropolar continua. *Journal of the Mechanics and Physics of Solids*, 127:62–79, 2019.
- [40] X. Ju, R. Mahnken, L. Liang, and Y. Xu. Goal-oriented mesh adaptivity for inverse problems in linear micromorphic elasticity. *Computers and Structures*, 257:106671, 2021.
- [41] S. Khakalo and J. Niiranen. Lattice structures as thermoelastic strain gradient metamaterials: Evidence from full-field simulations and applications to functionally step-wise-graded beams. *Composites Part B: Engineering*, 177:107224, 2019.
- [42] S. Khakalo and J. Niiranen. Anisotropic strain gradient thermoelasticity for cellular structures: Plate models, homogenization and isogeometric analysis. *Journal of the Mechanics and Physics of Solids*, 134:103728, 2020.
- [43] S. Khakalo, V. Balabanov, and J. Niiranen. Modelling size-dependent bending, buckling and vibrations of 2D triangular lattices by strain gradient elasticity models: Applications to sandwich beams and auxetics. *International Journal of Engineering Science*, 127:33–52, 2018.
- [44] H. Khan, I.-D. Ghiba, A. Madeo, and P. Neff. Existence and uniqueness of Rayleigh waves in isotropic elastic Cosserat materials and algorithmic aspects. *Wave Motion*, 110:102898, 2022.
- [45] R. C. Kirby, A. Logg, M. E. Rognes, and A. R. Terrel. Common and unusual finite elements. In *Automated Solution of Differential Equations by the Finite Element Method: The FEniCS Book*, pages 95–119. Springer Berlin Heidelberg, Berlin, Heidelberg, 2012.
- [46] D. Knees, S. Owczarek, and P. Neff. A local regularity result for the relaxed micromorphic model based on inner variations. to appear in *Journal of Mathematical Analysis and Applications*, 2022. doi: 10.48550/ARXIV.2208.04821. URL <https://arxiv.org/abs/2208.04821>.
- [47] J. Korelc and P. Wriggers. *Automation of Finite Element Methods*. Springer International Publishing, 2016.
- [48] A. Lahbazi, I. Goda, and J.-F. Ganghoffer. Size-independent strain gradient effective models based on homogenization methods: Applications to 3D composite materials, pantograph and thin walled lattices. *Composite Structures*, 284:115065, 2022.
- [49] R. S. Lakes. Cosserat shape effects in the bending of foams. *Mechanics of Advanced Materials and Structures*, 2022. doi: 10.1080/15376494.2022.2086328.
- [50] J.-H. Lee, J. P. Singer, and E. L. Thomas. Micro-/nanostructured mechanical metamaterials. *Advanced Materials*, 24(36):4782–4810, 2012.
- [51] T. Leismann and R. Mahnken. Comparison of hyperelastic micromorphic, micropolar and microstrain continua. *International Journal of Non-Linear Mechanics*, 77:115–127, 2015.
- [52] A. Li, Q. Wang, M. Song, J. Chen, W. Su, S. Zhou, and L. Wang. On strain gradient theory and its application in bending of beam. *Coatings*, 12(9), 2022.

- [53] C. Liebold and W. H. Müller. Comparison of gradient elasticity models for the bending of micromaterials. *Computational Materials Science*, 116:52–61, 2016.
- [54] A. Madeo, P. Neff, I.-D. Ghiba, L. Placidi, and G. Rosi. Band gaps in the relaxed linear micromorphic continuum. *Zeitschrift für angewandte Mathematik und Mechanik*, 95(9):880–887, 2015.
- [55] A. Madeo, P. Neff, M. V. d’Agostino, and G. Barbagallo. Complete band gaps including non-local effects occur only in the relaxed micromorphic model. *Comptes Rendus Mécanique*, 344(11-12):784–796, 2016.
- [56] A. Madeo, P. Neff, I.-D. Ghiba, and G. Rosi. Reflection and transmission of elastic waves in non-local band-gap metamaterials: a comprehensive study via the relaxed micromorphic model. *Journal of the Mechanics and Physics of Solids*, 95:441–479, 2016.
- [57] A. Madeo, P. Neff, G. Barbagallo, M. V. d’Agostino, and I.-D. Ghiba. A review on wave propagation modeling in band-gap metamaterials via enriched continuum models. In *Mathematical Modelling in Solid Mechanics*, volume 69 of *Advanced Structured Materials*, pages 89–105. Springer, Singapore, 2017.
- [58] R. D. Mindlin. Micro-structure in linear elasticity. *Archive for Rational Mechanics and Analysis*, 16:51–78, 1964.
- [59] R. D. Mindlin and N. N. Eshel. On first strain-gradient theories in linear elasticity. *International Journal of Solids and Structures*, 4(1):109–124, 1968.
- [60] J. C. Nédélec. Mixed finite elements in \mathbb{R}^3 . *Numerische Mathematik*, 35(3):315–341, 1980.
- [61] J. C. Nédélec. A new family of mixed finite elements in \mathbb{R}^3 . *Numerische Mathematik*, 50:57–81, 1986.
- [62] P. Neff. The Cosserat couple modulus for continuous solids is zero viz the linearized Cauchy-stress tensor is symmetric. *Zeitschrift für Angewandte Mathematik und Mechanik*, 86(11):892–912, 2006.
- [63] P. Neff, J. Jeong, I. Münch, and H. Ramézani. Linear Cosserat elasticity, conformal curvature and bounded stiffness. In *Mechanics of Generalized Continua: One Hundred Years After the Cosserats*, pages 55–63. Springer New York, 2010.
- [64] P. Neff, I.-D. Ghiba, A. Madeo, L. Placidi, and G. Rosi. A unifying perspective: the relaxed linear micromorphic continuum. *Continuum Mechanics and Thermodynamics*, 26(5):639–681, 2014.
- [65] P. Neff, I. D. Ghiba, M. Lazar, and A. Madeo. The relaxed linear micromorphic continuum: well-posedness of the static problem and relations to the gauge theory of dislocations. *The Quarterly Journal of Mechanics and Applied Mathematics*, 68(1):53–84, 2015.
- [66] P. Neff, B. Eidel, M. V. d’Agostino, and A. Madeo. Identification of scale-independent material parameters in the relaxed micromorphic model through model-adapted first order homogenization. *Journal of Elasticity*, 139:269–298, 2020.
- [67] S. Owczarek, I.-D. Ghiba, M. V. d’Agostino, and P. Neff. Nonstandard micro-inertia terms in the relaxed micromorphic model: well-posedness for dynamics. *Mathematics and Mechanics of Solids*, 24(10):3200–3215, 2019.
- [68] L. Placidi, E. Barchiesi, and A. Battista. An inverse method to get further analytical solutions for a class of metamaterials aimed to validate numerical integrations. In F. dell’Isola, M. Sofonea, and D. Steigmann, editors, *Mathematical Modelling in Solid Mechanics*, pages 193–210. Springer Singapore, Singapore, 2017.
- [69] H. Reda, S. E. Alavi, M. Nasimsobhan, and J.-F. Ganghoffer. Homogenization towards chiral Cosserat continua and applications to enhanced Timoshenko beam theories. *Mechanics of Materials*, 155:103728, 2021.
- [70] G. Rizzi, G. Hütter, A. Madeo, and P. Neff. Analytical solutions of the simple shear problem for micromorphic models and other generalized continua. *Archive of Applied Mechanics*, 91:2237–2254, 2021.
- [71] G. Rizzi, G. Hütter, A. Madeo, and P. Neff. Analytical solutions of the cylindrical bending problem for the relaxed micromorphic continuum and other generalized continua. *Continuum Mechanics and Thermodynamics*, 33:1505–1539, 2021.
- [72] G. Rizzi, H. Khan, I.-D. Ghiba, A. Madeo, and P. Neff. Analytical solution of the uniaxial extension problem for the relaxed micromorphic continuum and other generalized continua (including full derivations). *Archive of Applied Mechanics*, 2021. doi: 10.1007/s00419-021-02064-3.
- [73] G. Rizzi, M. V. d’Agostino, P. Neff, and A. Madeo. Boundary and interface conditions in the relaxed micromorphic model: Exploring finite-size metastructures for elastic wave control. *Mathematics and Mechanics of Solids*, 27(6):1053–1068, 2022.
- [74] G. Rizzi, G. Hütter, H. Khan, I.-D. Ghiba, A. Madeo, and P. Neff. Analytical solution of the cylindrical torsion problem for the relaxed micromorphic continuum and other generalized continua (including full derivations). *Mathematics and Mechanics of Solids*, 27(3):507–553, 2022.
- [75] G. Rizzi, P. Neff, and A. Madeo. Metamaterial for inner protection and outer tuning through a relaxed micromorphic approach. *Philosophical Transactions of the Royal Society A: Mathematical, Physical and Engineering Sciences*, 380(2231):20210400, 2022.
- [76] G. Rizzi, D. Tallarico, P. Neff, and A. Madeo. Towards the conception of complex engineering meta-structures: Relaxed-micromorphic modelling of low-frequency mechanical diodes/high-frequency screens. *Wave Motion*, 113:102920, 2022.
- [77] M. E. Rognes, R. C. Kirby, and A. Logg. Efficient assembly of $H(\text{div})$ and $H(\text{curl})$ conforming finite elements. *SIAM Journal on Scientific Computing*, 31(9):4130–4151, 2009.
- [78] O. Rokoš, M. M. Ameen, R. H. J. Peerlings, and M. G. D. Geers. Micromorphic computational homogenization for mechanical metamaterials with patterning fluctuation fields. *Journal of the Mechanics and Physics of Solids*, 123:119–137, 2019.

- [79] O. Rokoš, M. M. Ameen, R. H. J. Peerlings, and M. G. D. Geers. Extended micromorphic computational homogenization for mechanical metamaterials exhibiting multiple geometric pattern transformations. *Extreme Mechanics Letters*, 37:100708, 2020.
- [80] O. Rokoš, J. Zeman, M. Doškář, and P. Krysl. Reduced integration schemes in micromorphic computational homogenization of elastomeric mechanical metamaterials. *Advanced Modeling and Simulation in Engineering Sciences*, 7, 2020.
- [81] Z. Rueger, C. S. Ha, and R. S. Lakes. Cosserat elastic lattices. *Meccanica*, 54:1983–1999, 2019.
- [82] M. Sarhil, L. Scheunemann, P. Neff, and J. Schröder. On a tangential-conforming finite element formulation for the relaxed micromorphic model in 2D. *Proceedings in Applied Mathematics and Mechanics*, 21(1):e202100187, 2021.
- [83] F. Schmidt, M. Krüger, M.-A. Keip, and C. Hesch. Computational homogenization of higher-order continua. *International Journal for Numerical Methods in Engineering*, 123(11):2499–2529, 2022.
- [84] J. Schröder, M. Sarhil, L. Scheunemann, and P. Neff. Lagrange and $H(\text{curl}, \mathcal{B})$ based Finite Element formulations for the relaxed micromorphic model. *Computational Mechanics*, 2022. doi: 10.1007/s00466-022-02198-3.
- [85] N. Shekarchizadeh, B. E. Abali, E. Barchiesi, and A. M. Bersani. Inverse analysis of metamaterials and parameter determination by means of an automatized optimization problem. *Zeitschrift für Angewandte Mathematik und Mechanik*, 101(8):e202000277, 2021.
- [86] N. Shekarchizadeh, B. E. Abali, and A. M. Bersani. A benchmark strain gradient elasticity solution in two-dimensions for verifying computational approaches by means of the finite element method. *Mathematics and Mechanics of Solids*, 27(10):2218–2238, 2022.
- [87] F. Shi, N. Fantuzzi, P. Trovalusci, Y. Li, and Z. Wei. Stress field evaluation in orthotropic microstructured composites with holes as cosserat continuum. *Materials*, 15(18), 2022.
- [88] A. Skrzat and V. A. Eremeyev. On the effective properties of foams in the framework of the couple stress theory. *Continuum Mechanics and Thermodynamics*, 32:1779–1801, 2020.
- [89] A. Sky, M. Neunteufel, I. Münch, J. Schöberl, and P. Neff. A hybrid $H^1 \times H(\text{curl})$ finite element formulation for a relaxed micromorphic continuum model of antiplane shear. *Computational Mechanics*, 68:1–24, 2021.
- [90] A. Sky, M. Neunteufel, I. Münch, J. Schöberl, and P. Neff. Primal and mixed finite element formulations for the relaxed micromorphic model. *Computer Methods in Applied Mechanics and Engineering*, 399:115298, 2022.
- [91] A. Sridhar, V. G. Kouznetsova, and M. G. D. Geers. Homogenization of locally resonant acoustic metamaterials towards an emergent enriched continuum. *Computational Mechanics*, 57:423–435, 2016.
- [92] A. Sridhar, L. Liu, V. G. Kouznetsova, and M. G. D. Geers. Homogenized enriched continuum analysis of acoustic metamaterials with negative stiffness and double negative effects. *Journal of the Mechanics and Physics of Solids*, 119:104–117, 2018.
- [93] E. S. Suhubi and A. C. Eringen. Nonlinear theory of micro-elastic solids-II. *International Journal of Engineering Science*, 2(4):389–404, 1964.
- [94] J. U. Surjadi, L. Gao, H. Du, X. Li, X. Xiong, N. X. Fang, and Y. Lu. Mechanical metamaterials and their engineering applications. *Advanced Engineering Materials*, 21(3):1800864, 2019.
- [95] O. Weeger. Numerical homogenization of second gradient, linear elastic constitutive models for cubic 3D beam-lattice metamaterials. *International Journal of Solids and Structures*, 224:111037, 2021.
- [96] H. Yang and W. H. Müller. Size effects of mechanical metamaterials: a computational study based on a second-order asymptotic homogenization method. *Archive of Applied Mechanics*, 91:1037–1053, 2021.
- [97] H. Yang, B. E. Abali, D. Timofeev, and W. H. Müller. Determination of metamaterial parameters by means of a homogenization approach based on asymptotic analysis. *Continuum Mechanics and Thermodynamics*, 32:1251–1270, 2020.
- [98] H. Yang, D. Timofeev, B. E. Abali, B. Li, and W. H. Müller. Verification of strain gradient elasticity computation by analytical solutions. *Zeitschrift für Angewandte Mathematik und Mechanik*, 101(12):e202100023, 2021.
- [99] H. Yang, B. E. Abali, W. H. Müller, S. Barboura, and J. Li. Verification of asymptotic homogenization method developed for periodic architected materials in strain gradient continuum. *International Journal of Solids and Structures*, 238:111386, 2022.
- [100] S. Yin, Z. Xiao, Y. Deng, G. Zhang, J. Liu, and S. Gu. Isogeometric analysis of size-dependent Bernoulli-Euler beam based on a reformulated strain gradient elasticity theory. *Computers and Structures*, 253:106577, 2021.
- [101] X. Yu, J. Zhou, H. Liang, Z. Jiang, and L. Wu. Mechanical metamaterials associated with stiffness, rigidity and compressibility: A brief review. *Progress in Materials Science*, 94:114–173, 2018.
- [102] A. A. Zadpoor. Mechanical meta-materials. *Materials Horizons*, 3:371–381, 2016.
- [103] J. Zhi, L. H. Poh, T.-E. Tay, and V. B. C. Tan. Direct FE2 modeling of heterogeneous materials with a micromorphic computational homogenization framework. *Computer Methods in Applied Mechanics and Engineering*, 393:114837, 2022.
- [104] T. I. Zohdi and P. Wriggers. *An Introduction to Computational Micromechanics*. Springer Berlin, Heidelberg, 2005.